



University of
Massachusetts
Amherst

Rbc Lifespan Uncertainty: Models and Anemia Management Robustness

Item Type	Thesis (Open Access)
Authors	Dai, Rui
DOI	10.7275/4036016
Download date	2026-03-16 09:24:03
Link to Item	https://hdl.handle.net/20.500.14394/44458

**RBC LIFESPAN UNCERTAINTY: MODELS AND ANEMIA
MANAGEMENT ROBUSTNESS**

A thesis presented

by

RUI DAI

Submitted to the Graduate School of the
University of Massachusetts Amherst in partial fulfillment
of the requirements for the degree of
MASTER OF SCIENCE IN ELECTRICAL AND COMPUTER ENGINEERING
May 2013
Electrical & Computer Engineering

© Copyright by Rui Dai 2013

All Rights Reserved

RBC LIFESPAN UNCERTAINTY: MODELS AND ANEMIA
MANAGEMENT ROBUSTNESS

A Thesis Presented

By

RUI DAI

Approved as to style and content by:

Christopher V. Hollot, Chair

Yossi Chait, Member

Ted Djaferis, Member

Joseph Horowitz, Member

Christopher V. Hollot, Department Head
Electrical & Computer Engineering

To my beloved parents and all my friends

ABSTRACT

RBC LIFESPAN UNCERTAINTY: MODELS AND ANEMIA MANAGEMENT ROBUSTNESS

MAY 2013

RUI DAI

B.S. EAST CHINA JIAOTONG UNIVERSITY, CHINA

M.S.E.C.E UNIVERSITY OF MASSACHUSETTS AMHERST

Directed by: Professor Christopher V. Hollot

This thesis discusses the modeling of uncertainty of red blood cell (RBC) lifespan distribution in patients suffering from Chronic Kidney Disease (CKD) patients, whose anemia is managed through periodic dosing of erythropoietin (EPO).

In healthy individuals, RBCs containing hemoglobin (Hgb) are produced in the bone marrow. When oxygen carried by hemoglobin is transported to human tissues throughout the body, the kidneys sense reduced level of Hgb and secrete EPO that simulates proliferation of red cell precursors and eventually producing red blood cells. However, in CKD patients, their kidneys fail to secrete enough EPO, so that too few of RBCs are produced to maintain a sufficient Hgb level. As a result, artificial EPO dosing is required when the kidney loses this function to avoid anemia.

To develop effective artificial EPO dosing schemes, it is important to have models of how EPO does dynamically affect hemoglobin levels. Since there is significant uncertainty in this process, it is equally valuable to have mathematical models of such uncertainties, and in this thesis we focus on uncertainty in the lifespan of red blood cells.

In this thesis, we consider two different types of models for RBC lifespan uncertainty: the time-invariant and time-varying cases. In the former, we treat the probabilistic distribution of cell lifespans as fixed for a given patient, but variable (uncertain) over the population. In the latter case, the cell lifespan distribution can change from moment to moment for a given patient.

Amongst several possible choices of RBC lifespan distributions, this thesis will focus on the gamma distribution. For the time-invariant model, a first-order gamma distribution is selected as the nominal distribution, and a multiplicative error model is proposed to analyze the impact of lifespan uncertainty on anemia management.

In the time-varying case, the lifespan distribution is not fixed in time, but allowed to switch over a finite collection of gamma distributions. In other words, each newly-born RBC has a lifespan coming from a distribution chosen from a collection. Both of these models are analyzed so as to evaluate the impact of lifespan uncertainty on the performance of anemia management schemes; including stability and response time.

TABLE OF CONTENTS

	Page
ABSTRACT	v
LIST OF FIGURES	ix
CHAPTER	
1 INTRODUCTION	1
1.1 Backgrounds	1
1.1.1 Erythropoiesis	1
1.1.2 Role of kidney	2
1.2 Model of an AMCS	3
1.3 RBC dynamics.....	4
1.3.1 Compartmental model	4
1.3.2 Transfer function of RBC pool.....	6
1.4 Properties of the RBC pool.....	7
1.4.1 DC gain of $H(s)$	7
1.4.2 Stability of $H(s)$	8
1.4.3 Frequency response of $H(s)$	9
1.5 Thesis Motivation.....	11
1.6 Thesis contributions.....	12
2 SIMPLIFIED ANEMIA MANAGEMENT MODEL	14
2.1 PK/PD model.....	14
2.1.1 Introduction	14
2.1.2 Approximating the pulsatile nature of PK/PD.....	15
2.2 Iron, blood volume and endogenous EPO	16
2.3 Continuous-time model of AMCS.....	17
2.3.1 Sampled-data control system.....	17
2.3.2 Continuous-time approximation	18
2.3.3 Illustration	23
3 UNCERTAINTY IN RBC POOL DYNAMICS (TIME-INVARIANT CASE)	26
3.1 Lifespan distributions	27
3.1.1 Properties of lifespan distribution	27
3.1.2 Examples of lifespan distributions	28
3.2 Time-invariant uncertainty model and robustness.....	29
3.2.1 Multiplicative error model.....	30
3.2.2 Robust stability	31

3.3 Error bounds	33
3.3.1 A multiplicative error bound	33
3.3.2 Conjectured tighter bound	35
3.4 Robust stability	36
3.5 Robust performance.....	38
4 UNCERTAINTY IN RBC POOL DYNAMICS (TIME-VARYING CASE).....	42
4.1 Time-varying lifespan distributions	42
4.2 RBC dynamics for time-varying lifespan distributions	43
4.3 The AMCS	44
4.4 Quadratic stability	48
4.5 Robust performance analysis and examples.....	51
4.5.1 Robust performance.....	51
4.5.2 Illustrative example	53
4.5.3 Impact of parameters of lifespans and controller	56
5 CONCLUSIONS.....	62
APPENDIX: PROOF FOR THEOREM 3.1.....	65
BIBLIOGRAPHY	70

LIST OF FIGURES

Figure	Page
1.1: Erythropoiesis (copied from [2])	2
1.2: The feedback control loop of an AMCS	3
1.3: RBC pool dynamic.....	4
1.4: Frequency response of $H(j\omega)$	11
2.1: PK/PD model	14
2.2: RBC production rate	15
2.3: T-averaging of RBC production rate	16
2.4: PK/PD model approximation.....	16
2.5: sampled-data system	17
2.6: Sampling model	19
2.7: Impulse-modulation model for sampling.....	20
2.8: Impulse-modulation model for sampling (frequency domain).....	21
2.9: A simplified system	22
2.10: Simplified continuous-time system	22
2.11: Simulink simulation for simplified sampled-data system.....	24
2.12: Simulation for approximated continuous-time system	24
2.13: Comparison of two systems	25
3.1: Perturbed model with multiplicative error.....	30
3.2: AMCS with perturbed RBC pool dynamic.....	32
3.3: Verification of Theorem 3.1 for $\bar{\tau} = 100$ and $k = 2, 3, \dots, 100$	35
3.4: Matlab example of the conjecture for $k = 2, 3, \dots, 10000$	36
3.5: Robust stability for LTI case	37
3.6: Implication on control design	38
3.7: Nominal performance of AMP	40

3.8: Robust performance for the time-invariant system.....	41
4.1: Time-varying RBC pool with sub-pools.....	44
4.2: Simplified state-space model of AMP system.....	45
4.3: Time-varying model of RBC pool with two potential lifespans.....	46
4.4: Performance with decay rate.....	48
4.5: AMCS time constant $\left(\frac{1}{\alpha}\right)$ vs. pool mean lifespan $(\bar{\tau}_1)$ parameterized by gain of the PI-AMP (K)	57
4.6: distribution of AMCS time constant $\left(\frac{1}{\alpha}\right)$ parameterized over pool mean lifespan $(\bar{\tau})$ and order of lifespan distribution (k)	58
4.7: distribution of AMCS time constant $\left(\frac{1}{\alpha}\right)$ parameterized over pool mean lifespan $(\bar{\tau})$, order of lifespan distribution (k) and PI-AMP gain (K)	61
A.1: Matlab example of the loser conjecture $(k = 2, 3, \dots, 100)$	69

CHAPTER 1

INTRODUCTION

In this chapter, we first introduce some background of erythropoiesis and anemia, and then introduce a model of an Anemia Management control system (AMCS). We also introduce the dynamics of the red blood cell (RBC) pool which is the focus of the thesis. Finally, we conclude this introductory chapter with the motivation and contributions of this thesis.

1.1 Backgrounds

To understand an AMCS, two biological phenomena are introduced: the production of RBCs, which is called erythropoiesis, and the role of the kidneys in hemoglobin (Hgb) regulation.

1.1.1 Erythropoiesis

One of the major functions of red blood cells is the exchange of oxygen and carbon dioxide; i.e., the transport of oxygen to tissues and of carbon dioxide (CO_2) back to the lungs [1]. Red blood cells are capable of carrying oxygen because they contain the protein hemoglobin which attracts oxygen in circulation. Hemoglobin contains four molecules, each of which has an iron atom in the middle. It is these iron atoms which attract oxygen and which make Hgb the oxygen carrier. Hgb concentration is a key measure of the oxygen level in the blood. It is said that Hgb occupies one third of the mass of RBCs [1], which gives a relationship that links the mass of Hgb and to the amount of RBCs.

The process of red blood cell formation is called erythropoiesis. In a healthy human, stem cells in the red bone marrow divide into two daughter cells, one of which matures into a red blood cell upon receiving the hormone erythropoietin (EPO), the other will become a new stem cell. Generally speaking, this daughter stem cell evolves through four stages; EPO and iron are needed in the process. As it grows into a RBC precursor cell in the bone marrow, it produces more and more Hgb. When

there is enough hemoglobin, the cell is released into the blood stream as a mature red blood cell. When an RBC passes through the lungs, oxygen binds to Hgb and is then carried by the cell throughout the body. Figure 1.1 shows the process from stem cell to red blood cells in circulation [2].

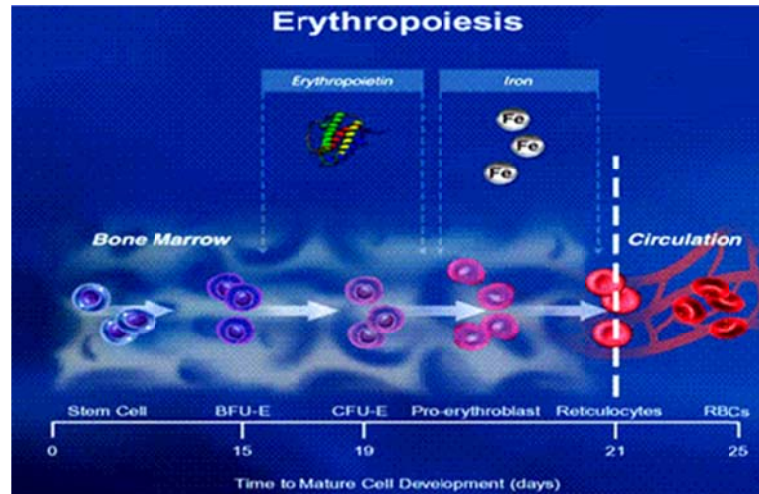


Figure 1.1: Erythropoiesis (copied from [2])

1.1.2 Role of kidney

The kidney has two functions in this oxygen balance: one is to sense the blood oxygen level; while the second is to secrete EPO to generate RBCs. When oxygen carried by RBCs (specifically hemoglobin molecules) is consumed by tissues, the kidney senses the decreased oxygen and then secretes EPO (a small fraction of EPO is also secreted by the liver) to simulate proliferation of red cell precursors to produce more RBCs – to increase Hgb mass - and to increase the blood oxygen level.

However, for chronic kidney disease (CKD) patients, the kidneys fail to secrete enough EPO. In turn, fewer stem cells in the bone marrow mature to RBC precursors. This is the reason why CKD patients have low RBC counts; anemia is a very common condition in these patients.

The World Health Organization defines anemia as “a hemoglobin concentration lower than 13.0 g/dL in men and postmenopausal women and lower than 12.0 g/dL in other women” [3]. As a common complication in advanced chronic kidney disease, anemia has many causes, but is related largely to decreased production of EPO by

diseased kidneys [4]. In order to maintain acceptable levels of Hgb concentration, this lost kidney function needs to be compensated. The discovery of recombinant human EPO (rHuEPO) in 1989, which has the same biological effects as endogenous erythropoietin (EPO secreted by the kidney), has led to its use as a treatment of anemia in chronic renal failure patients [5]. However, the appropriate size and frequency of doses remains a challenge [29]. This is why a study of an AMCS is necessary.

1.2 Model of an AMCS

In the previous section, we briefly reviewed the biology and the feedback interaction of the kidney and erythropoiesis. Now we focus on an anemia management protocol (AMP), as the control element in an AMCS.

In a healthy individual, the kidney and erythropoiesis form a feedback control system to regulate Hgb levels. In CKD patients, an AMP replaces the kidney, acting as the controller in an AMCS feedback loop where erythropoiesis is the process to be controlled and where Hgb is the primary performance and measured variable. This feedback loop is closed during periodic dialysis treatments (typically three times weekly) when a patient's hemoglobin is measured and, accordingly, the AMP prescribes EPO doses as compensatory action. The thesis is motivated by model-based AMP design and with the feedback control system developed in [6, 7, 8] as shown in Figure 1.2.

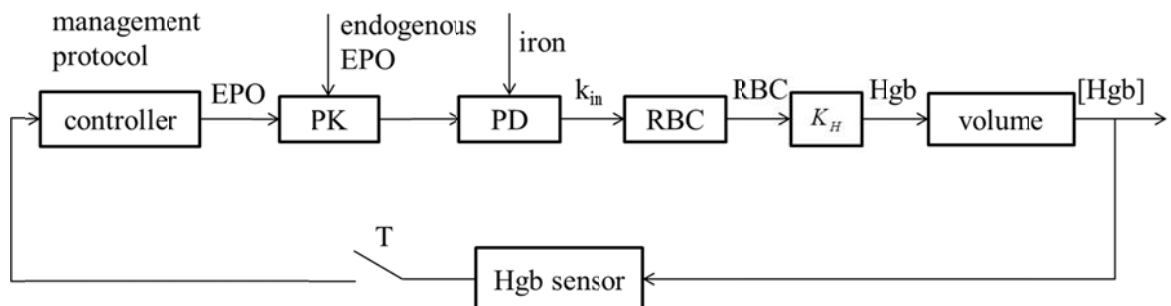


Figure 1.2: The feedback control loop of an AMCS

In this figure, PK (pharmacokinetics) models the dynamics of intravenous EPO dosing, including residual EPO secretion from the compromised kidneys (endogenous

EPO), while PD (pharmacodynamics) models EPO's effect on red blood cell production. Following [6 - 8], PK and PD are modeled by

$$\dot{E}(t) = -\frac{V_{\max} E(t)}{K_m + E(t)} + \sum_{i=0}^{\frac{t}{T}} EPO_i \delta(t - iT)$$

$$k_{in}(t) = \frac{S(E(t) + E_{en}(t))}{C + E(t) + E_{en}(t)}$$

where E denotes exogenous EPO plasma levels, E_{en} endogenous EPO, EPO_i the i th EPO dose, T_s the sampling period as well as the dosing period, and k_{in} the production rate of mature red blood cells. The differential and production equations employ saturating functions with parameters V_{\max} , K_m , S and C . Finally, the blood volume comes into play since the sensor reports on Hgb concentration, which is represented by [Hgb] in Figure 1.2.

1.3 RBC dynamics

The anemia management system in Figure 1.2 has been purposely simplified to focus on the RBC pool dynamics and, as the main theme of this thesis proposal, on model uncertainty and its impact on feedback loop performance. In this section we introduce a basic model of this pool dynamic.

1.3.1 Compartmental model

In order to study the RBC pool dynamic, the input of the RBC pool is “averaged” to derive a continuous-time form of this input [7]. Consider the RBC pool dynamic in Figure 1.3, with input $\bar{k}_{in}(t)$ and output $Hgb(t)$ which respectively denote the rate of newly-born red blood cells and the total number of RBCs in the blood pool.

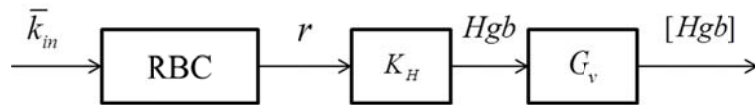


Figure 1.3: RBC pool dynamic

The RBC pool dynamic can be treated as a compartmental model, defined by the law of mass conservation, where the rate of newly-formed RBCs $\bar{k}_{in}(t)$ forms the pool's input stream and the rate of eliminated RBCs $k_{out}(t)$ forms the pool's output stream; and where their difference determines the rate of change in the number of RBCs presently in the pool, see Figure 1.3. Also, let K_H denote the linear relationship between RBCs and Hgb. After taking into consideration the blood volume, the output of the RBC pool is Hgb concentration, denoted by $[Hgb]$. Let $r(t)$ denote the number of RBCs, then we get

$$\dot{r}(t) = \bar{k}_{in}(t) - k_{out}(t)$$

and

$$[Hgb](t) = G_v K_H r(t).$$

The elimination rate $k_{out}(t)$ can be expressed in terms of RBC lifespan τ , the time from a cell's birth to death, and the time-varying distribution of such lifespans $l(t, \tau)$; i.e., at time t , newly-born RBCs have lifespans τ each chosen from the lifespan distribution (pdf) $l(t, \tau)$. From [6, 13], the elimination rate satisfies

$$k_{out}(t) = \int_0^t \bar{k}_{in}(t - \tau) l(\tau, t - \tau) d\tau$$

and when the RBC lifespan distribution is time-independent, i.e., $l(t, \tau) \equiv l(\tau)$, then the above becomes the convolution

$$k_{out}(t) = \int_0^t \bar{k}_{in}(t - \tau) l(\tau) d\tau \triangleq (\bar{k}_{in} * l)(t).$$

As shown in Figure 1.2, we will focus on this simplified system and the uncertainty which comes into play in the RBC pool.

The RBC pool dynamics directly relate $\bar{k}_{in}(t)$ to $r(t)$ can be expressed as either

$$\dot{r}(t) = \bar{k}_{in}(t) - \int_0^t \bar{k}_{in}(t - \tau) l(\tau, t - \tau) d\tau$$

when the lifespan distribution is time-varying, or as

$$\dot{r}(t) = \bar{k}_{in}(t) - (\bar{k}_{in} * l)(t),$$

when it's time-invariant. We will refer to the former as the time-varying case, and the latter as the time-invariant model. The study of these two models, as it relates to an AMCS is the focus of this thesis.

1.3.2 Transfer function of RBC pool

From Section 1.3.1, the general RBC pool equation in the time-invariant case is:

$$\dot{r}(t) = \bar{k}_{in}(t) - (\bar{k}_{in} * l)(t); \quad r(0) = r_0, t \geq 0$$

where $r(t)$ denotes the number of RBCs in the pool. Recall that $[Hgb](t) = G_v K_H r(t)$. We now assume the blood volume is constant, and $K_H \approx \frac{1}{3}$. For simplicity, we take $K_H = G_v = 1$ and as a result, have that the output of the RBC pool to be $[Hgb]$. Furthermore, from now on, we will use $Hgb(t)$ to represent the concentration $[Hgb]$. Thus,

$$\dot{Hgb}(t) = \bar{k}_{in}(t) - \int_0^t \bar{k}_{in}(t-\tau)l(\tau)d\tau; \quad Hgb(0) = Hgb_0, t \geq 0$$

To compute the transfer function of the above system, we assume that the system is at rest, implying that $Hgb_0 = 0$. To compute this transfer function we first take the Laplace transform of both sides of the above to obtain

$$s \cdot Hgb(s) = K_{in}(s) - K_{in}(s) \cdot L(s)$$

where $K_{in}(s)$, $Hgb(s)$ and $L(s)$ denote the Laplace transform of $\bar{k}_{in}(t)$, $Hgb(t)$ and $l(\tau)$ respectively with

$$H(s) \triangleq \frac{Hgb(s)}{K_{in}(s)}$$

it is clear that

$$H(s) = \frac{K_{in}(s)[1-L(s)]}{s \cdot K_{in}(s)} = \frac{1-L(s)}{s}.$$

1.4 Properties of the RBC pool

Having derived the transfer function for the RBC pool dynamic, we are now in a position to analyze the frequency response of the RBC pool. This frequency response is useful in frequency-domain based design of AMCS.

1.4.1 DC gain of $H(s)$

The DC gain of transfer function $H(s)$ is given by

$$DC \text{ gain} \triangleq H(s)\Big|_{s=0},$$

a transfer function's DC gain describes a system's steady-state response to a constant input.

From the definition of Laplace transform,

$$L(s)\Big|_{s=0} = \int_0^{\infty} l(\tau)e^{-s\tau} d\tau \Big|_{s=0} = \int_0^{\infty} l(\tau)d\tau = 1.$$

Applying l'Hôpital's rule we get

$$H(0) = \frac{1-L(s)}{s} \Big|_{s=0} = \frac{0-L'(s)}{1} \Big|_{s=0} = -L'(0).$$

Applying the definition of the Laplace transform again, the derivative of $L(s)$ is given by

$$-L'(0) = -\frac{d}{ds} \int_0^{\infty} l(\tau)e^{-s\tau} d\tau \Big|_{s=0} = -\int_0^{\infty} \frac{\partial}{\partial s} [e^{-s\tau} l(\tau)] d\tau \Big|_{s=0},$$

where here the interchange of differentiation and integration is valid.

Thus,

$$\begin{aligned} H(s)\Big|_{s=0} &= \frac{0-L'(s)}{1} \Big|_{s=0} \\ &= -\int_0^{\infty} \frac{\partial}{\partial s} [e^{-s\tau} l(\tau)] d\tau \Big|_{s=0} \\ &= \int_0^{\infty} e^{-s\tau} \tau l(\tau) d\tau \Big|_{s=0} \\ &= \int_0^{\infty} \tau l(\tau) d\tau. \end{aligned}$$

Recognizing that $\bar{\tau} \triangleq \int_0^{\infty} \tau l(\tau) d\tau$ which is the mean of the lifespan distribution function, then the DC gain is given by:

$$\text{DC gain} = H(0) = \bar{\tau}.$$

This computation holds for any lifespan distribution having a Laplace transform.

1.4.2 Stability of $H(s)$

As discussed in Section 1.3, the transfer function of the RBC pool is given by

$$H(s) = \frac{1 - L(s)}{s},$$

where $L(s)$ is the Laplace transform of $l(\tau)$. We now focus on the family of gamma distributions [6] so that

$$l(\tau; k, \bar{\tau}) = \frac{k^k}{\bar{\tau}^k} \frac{1}{\Gamma(k)} \tau^{k-1} e^{-\frac{k\tau}{\bar{\tau}}}; \quad \tau \geq 0, k, \bar{\tau} > 0,$$

with Laplace transform

$$L(s) = \frac{1}{\left(1 + \frac{\bar{\tau}}{k}s\right)^k}; \quad \bar{\tau} \geq 0, k = 1, 2, \dots,$$

The parameter k denotes the order, which is a positive integer. It is clear that $L(s)$ has k repeated poles at $s = -\frac{k}{\bar{\tau}} < 0$, so $L(s)$ has all its poles in the left-half of the complex plane.

For a continuous linear time-invariant system, bounded-input bounded-output (BIBO) stability is equivalent to the impulse response being absolutely integrable, which in turn, is equivalent to the transfer function having all its poles in the open left-half plane.

Since $H(s) = \frac{1 - L(s)}{s}$ and from Section 1.4.1 $H(0) = \bar{\tau}$, we conclude that the poles of $H(s)$ are precisely those of $L(s)$. Hence $H(s)$ is BIBO stable. However, since $\frac{1 - L(s)}{s}$ has a pole-zero cancellation at $s = 0$, then the RBC pool dynamic is not asymptotically stable. However, it is stable in the sense of Lyapunov [32].

1.4.3 Frequency response of $H(s)$

We now give an upper bound to the magnitude frequency response $|H(j\omega)|$.

The first bound is

$$|H(j\omega)| \leq \frac{2}{\omega}.$$

To see this we compute

$$|H(j\omega)| = \left| \frac{1-L(j\omega)}{j\omega} \right| = \frac{|1-L(j\omega)|}{|j\omega|} = \frac{|1-L(j\omega)|}{\omega},$$

from which subadditivity gives

$$\frac{|1-L(j\omega)|}{\omega} \leq \frac{1+|L(j\omega)|}{\omega}.$$

From the Laplace transform,

$$\frac{1+|L(j\omega)|}{\omega} = \frac{1+\left|\int_0^\infty l(\tau)e^{-j\omega\tau}d\tau\right|}{\omega} \leq \frac{1+\int_0^\infty l(\tau)|e^{-j\omega\tau}|d\tau}{\omega}.$$

This inequality holds because $l(\tau)$ is non-negative. Since $|e^{-j\omega\tau}|=1$ and

$\int_0^\infty l(\tau)d\tau=1$, then

$$\frac{1+\int_0^\infty l(\tau)|e^{-j\omega\tau}|d\tau}{\omega} = \frac{1+\int_0^\infty l(\tau)d\tau}{\omega} = \frac{2}{\omega}.$$

As a result,

$$|H(j\omega)| \leq \frac{1+|L(j\omega)|}{\omega} \leq \frac{2}{\omega}.$$

Now we show that $|H(j\omega)| \leq \bar{\tau}$. Indeed,

$$\begin{aligned}
|H(j\omega)| &= \frac{|1 - L(j\omega)|}{\omega} \\
&= \frac{\left| \int_0^\infty l(\tau) d\tau - \int_0^\infty l(\tau) e^{-j\omega\tau} d\tau \right|}{\omega} \\
&= \frac{\left| \int_0^\infty l(\tau) (1 - e^{-j\omega\tau}) d\tau \right|}{\omega}.
\end{aligned}$$

Since $l(\tau)$ is non-negative,

$$\frac{\left| \int_0^\infty l(\tau) (1 - e^{-j\omega\tau}) d\tau \right|}{\omega} \leq \frac{\int_0^\infty l(\tau) |1 - e^{-j\omega\tau}| d\tau}{\omega}.$$

Because $e^{-j\omega\tau} = \cos(\omega\tau) - j \sin(\omega\tau)$, one obtains

$$\begin{aligned}
|1 - e^{-j\omega\tau}| &= |1 - [\cos(\omega\tau) - j \sin(\omega\tau)]| \\
&= \sqrt{2 - 2 \cos(\omega\tau)} \\
&= 2 \sin \left| \frac{\omega\tau}{2} \right| \leq \omega\tau; \quad \omega \geq 0, \tau \geq 0.
\end{aligned}$$

Then,

$$\frac{\int_0^\infty l(\tau) \cdot 2 \sin \left| \frac{\omega\tau}{2} \right| d\tau}{\omega} \leq \frac{\int_0^\infty l(\tau) \cdot \omega\tau d\tau}{\omega}.$$

The right side of this inequality can be further simplified as

$$\frac{\int_0^\infty l(\tau) \cdot \omega\tau d\tau}{\omega} = \frac{\omega \int_0^\infty l(\tau) \tau d\tau}{\omega} = \bar{\tau}.$$

As a result:

$$|H(j\omega)| \leq \frac{\int_0^\infty l(\tau) |1 - e^{-j\omega\tau}| d\tau}{\omega} \leq \frac{\int_0^\infty l(\tau) \cdot \omega\tau d\tau}{\omega} = \bar{\tau}.$$

Figure 1.4 shows the magnitude Bode plot of the RBC pool; the lifespan distribution is taken as first-order gamma, with a mean lifespan of 100 days. Note that the upper bounds intersect $\omega = \frac{2}{\bar{\tau}}$. Clearly then, $H(s)$ has a low-pass frequency response with corner frequency less than $\frac{2}{\bar{\tau}}$ days. This result holds for all lifespan distributions.

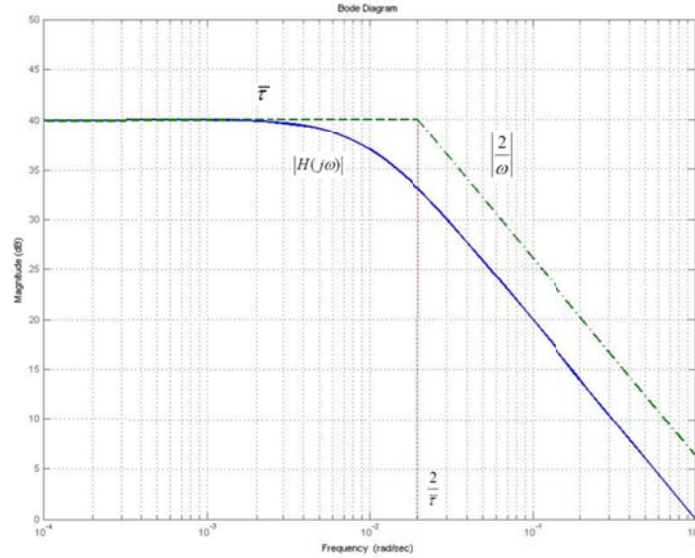


Figure 1.4: Frequency response of $H(j\omega)$

1.5 Thesis Motivation

There are several factors that influence regulation of Hgb levels, and uncertainty in RBC lifespan distribution may be one of the prominent factors.

Wojciech Krzyzanski et al [6] proposed lifespan-based response models, which included comparisons of several probability density functions. However, these simulations were based on perfect knowledge of the lifespan distributions.

Although several potential lifespan distribution functions have been proposed and analyzed, the real RBC lifespan remains unknown. There is no rule of which type of probability density function it should be, so it is difficult to determine whether or not any particular protocol design is able to achieve the target Hgb concentration level, even if all the other elements in the system are simplified and fixed. An AMP may result in good AMCS performance for one particular distribution; but very possibly it may not be capable to work with another distribution. It is thus necessary to determine the effectiveness of the anemia management protocol, taking into consideration that the RBC lifespan distribution may vary among the population or vary within an individual over time.

The objective in designing an anemia management protocol is to maintain Hgb level within a target range. Unknown RBC lifespan distributions and AMCS

performance may be influenced by their possible impact. As a result, there is need to study the impact of uncertainty in lifespan distribution, which is the motivation of this thesis. We will provide models for such uncertainty and analyze AMCS performance in the face of these uncertainties.

1.6 Thesis contributions

The major contribution of this thesis is to develop two models of RBC lifespan uncertainty, so that the robustness and performance of the AMCS can be analyzed. Our results provide methods to evaluate and aid in the design of an AMP.

Consider the RBC pool as a compartmental model, the dynamics are studied based on the transfer function derived from the general differential equation. Results indicate that the RBC pool is BIBO stable with a steady-state response related to the mean lifespan.

The focus on lifespan uncertainty is based on the family of gamma distributions. Both the time-invariant and time-varying models of lifespan uncertainty are derived from the general differential equation.

The time-invariant model for the RBC lifespan distribution uncertainty allows lifespan variations amongst the population. We chose a nominal model of the RBC pool with first-order gamma distribution, and then conjectured a bound on the multiplicative error of the RBC pool. Although the mathematical proof for the bound is still open, we provided another weaker bound which is proved. These bounds are used to provide constraints on the design of the AMP so as to achieve robustness of the system.

Uncertainty of RBC lifespan varying over time is studied by the time-varying model. Each red blood cell chooses a lifespan distribution from a pre-determined collection of time-invariant gamma distributions, and the separation of this lifespan generates a standard form of the system with a set of time-invariant sub-pools and an arbitrary switching signal. We analyzed the impact of the AMP's gain and the two parameters (order and mean lifespan) of gamma distributions via Matlab's LMI toolbox. Results show that mean lifespan within a certain range will not have much

effect on the stability of the system, and increasing PI-AMP gain leads to faster response, however, large order of gamma distributions may result in loss of stability.

CHAPTER 2

SIMPLIFIED ANEMIA MANAGEMENT MODEL

In this chapter, we introduce a simplified model of anemia management that will be used in the remainder of the thesis. These simplifications allow the original model in Figure 1.2, which is nonlinear and hybrid-time, containing both continuous and discrete-time components, to be expressed in terms of linear, continuous-time elements. This will allow for standard uncertainty modeling and robust feedback results to be employed.

2.1 PK/PD model

Due to the discrete-time nature of EPO dosing, and the nature of nonlinear PK/PD dynamics, the rate at which new RBCs are produced is pulsatile in time. Given the low-pass nature of the anemia management feedback system in general, and the RBC pool in particular, the high-frequency components of these pulses are filtered out, leaving the average-value of PK/PD dynamics' output as the significant driving signal of this loop. In this section, we will consider this PK/PD model and explain the technique of “averaging” introduced in [7], to arrive at a linear sampled-data model for the AMCS (Anemia Management Control System).

2.1.1 Introduction

As introduced in Chapter 1, the PK/PD model describes the rate at which RBCs are produced due to the instigation of EPO doses. Figure 2.1 illustrates this system where the

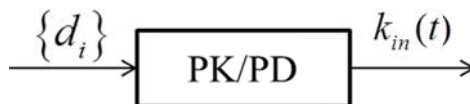


Figure 2.1: PK/PD model

intravenous rHuepo doses are denoted by d_i , where i presents the i -th dose and where the production rate of RBCs is $k_{in}(t)$. From [6, 7] the PK/PD dynamics are modeled by the differential equations:

$$\dot{E}(t) = -\frac{V_{\max} E(t)}{K_m + E(t)} + \sum_{i=0}^{\lfloor \frac{t}{T_s} \rfloor} d_i \delta(t - iT_s); \quad E(0) = E_0$$

$$k_{in}(t) = \frac{S_{\max} (E + E_N)}{SC_{50} + (E + E_N)}$$

where $E(t)$ is the level of plasma EPO due to the dosing, and E_N is EPO's endogenous level. Both the differential and output equation use saturating functions with parameters V_{\max} , K_m , S_{\max} and SC_{50} as defined in [7].

2.1.2 Approximating the pulsatile nature of PK/PD

As mentioned, the output $k_{in}(t)$ of the PK/PD dynamic is pulsatile, even when the dosing regimen is constant, and now we discuss approximating these pulses by a piecewise constant signal representing the average of $k_{in}(t)$ over the dosing period T_s .

Suppose $k_{in}(t)$ evolves as illustrated in Figure 2.2(b), due to the dosing in Figure 2.2(a).

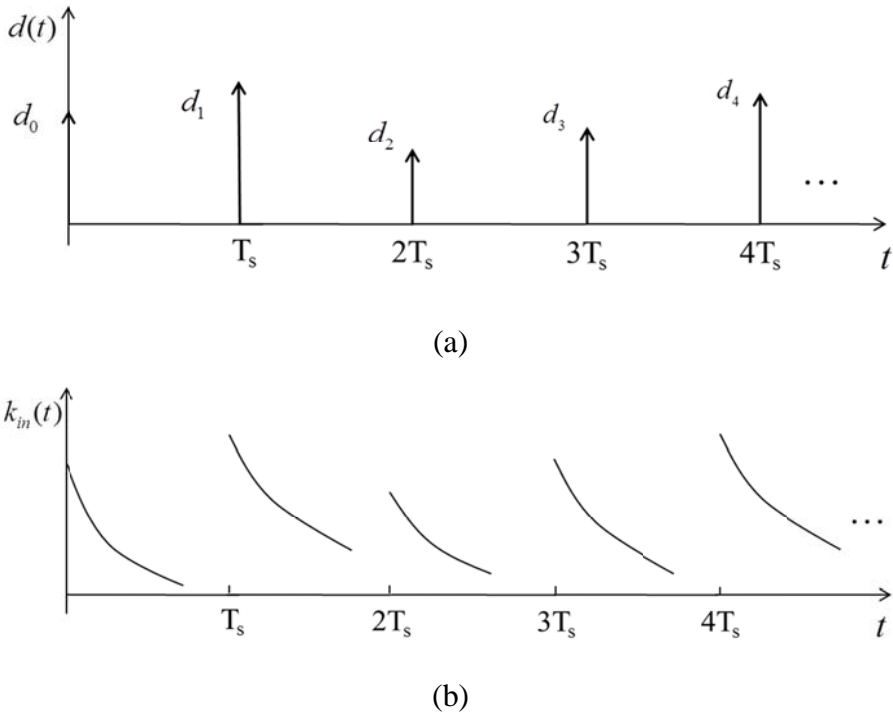


Figure 2.2: RBC production rate

In Figure 2.3 we give a zero-order approximation to the pulses in Figure 2.2(b) where

$$k_{avg}(d_i) \triangleq \frac{1}{T_s} \int_{iT_s}^{(i+1)T_s} k_{in}(t) dt,$$

and $\bar{k}_{in}(t)$ is defined by

$$\bar{k}_{in}(t) \triangleq \sum_{i=0}^{\infty} k_{avg}(d_i) \{u(t - iT_s) - u[t - (i+1)T_s]\}.$$

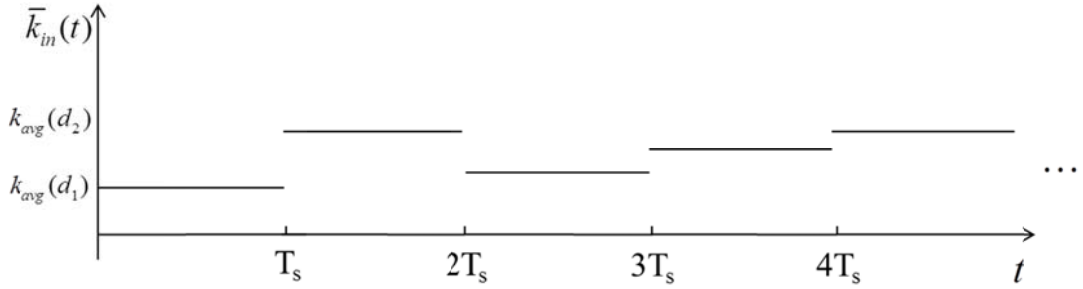


Figure 2.3: T-averaging of RBC production rate

The technique of “averaging” used in approximating $k_{avg}(d_i)$ has been computed in [7]. A block diagram representative for the relationship between EPO dose d_i and \bar{k}_{in} is shown in Figure 2.4.

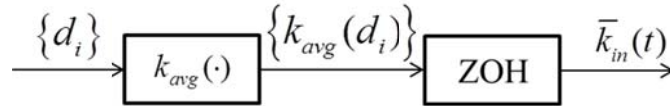


Figure 2.4: PK/PD model approximation

2.2 Iron, blood volume and endogenous EPO

In an anemia management system, four factors influence the Hgb concentration – as seen in Figure 1.2 – the iron required to form the Hgb molecules, blood volume which will affect the concentration of Hgb, the amount of endogenous EPO produced by the kidneys, and the exogenous EPO.

While iron supplements are necessary to meet the demands of erythropoiesis [9, 10], there is no evidence showing that iron intake causes change to Hgb concentration. In this thesis we will assume the iron pool is constant. The blood volume is also

considered constant. A study in [11] shows that even if there is a possible change of blood volume, it occurs much faster than the process of erythropoiesis. So it is reasonable to assume a constant blood volume for simplicity.

As no literature and research indicate the endogenous EPO level with exact data, we assume that the secreted endogenous EPO is constant for simplicity.

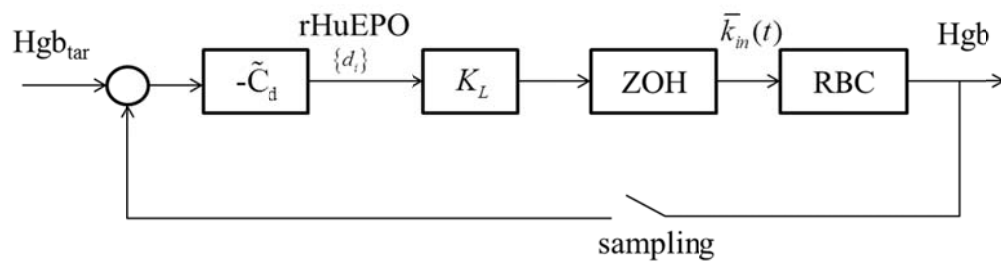
These assumptions are made for a simplified system, of which the focus is the RBC pool and its lifespan uncertainty.

2.3 Continuous-time model of AMCS

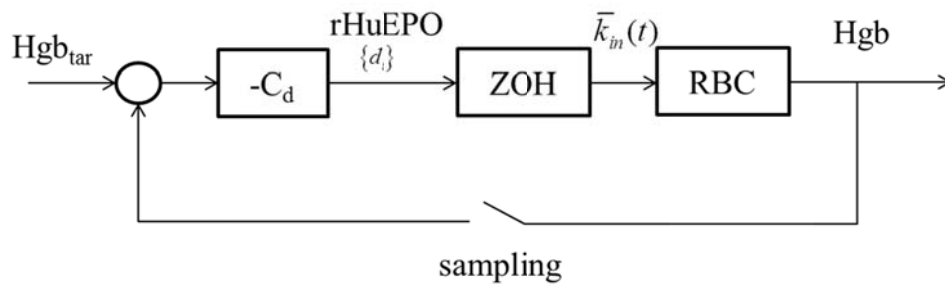
The assumptions discussed in previous section lead to an AMCS modeled as a sampled-data control system. In this section we will approximate it by a continuous-time system since this is a natural domain to model uncertainty in the RBC pool dynamics.

2.3.1 Sampled-data control system

Under the assumptions made in Section 2.2, the AMCS can be represented as in Figure 2.5.



(a)



(b)

Figure 2.5: sampled-data system

In Figure 2.5(a), the linearized K_L is the linearization of k_{avg} around a nominal dose d_0 ,

$$K_L = \left. \frac{d}{dr} k_{avg}(r) \right|_{r=d_0} \approx 1,$$

notice that this assumption is not based on the real system, but totally for simplicity. Now the system is further simplified as shown in Figure 2.5 (b).

The Hgb concentration is measured periodically, which we assume to be once per week. Samples of Hgb are used by the management protocol; the protocol, represented as the controller transfer function C_d is discrete-time. As shown in Figure 2.5, the protocol and the sampler comprise the discrete-time components of the feedback system, while the other models are continuous-time. This is an example of sampled-data control system which includes both discrete-time and continuous-time signals and system. Next, we will approximate this sampled-data control system by a continuous-time feedback version.

2.3.2 Continuous-time approximation

In this section, we approximate the sampled-data system by accounting for the sampler, discrete-time controller and the zero-order hold.

From Figure 2.5, the AMC consists of a sampler, where the signal Hgb is sampled at discrete instants, i.e., every seven days. The Nyquist sampling theorem [12] gives conditions on the sampling period T_s under which the continuous-time signal $Hgb(t)$ can theoretically be reconstructed from its samples $\{Hgb(kT_s)\}$. It is under such condition that we will approximate the sampled-data model of an AMCS.

To develop this approximation, we first consider the sampling functions

$$p_{T_s}(t) = \sum_{n=0}^{\infty} \delta(t - nT_s),$$

where $\delta(t)$ is the unit impulse and where the Fourier transform of $p_{T_s}(t)$ is

$$P_{T_s}(j\omega) = \frac{2\pi}{T_s} \sum_{k=-\infty}^{\infty} \delta\left(\omega - \frac{2k\pi}{T_s}\right).$$

In Figure 2.6 we reframe the sampled-data AMCS using $p_{T_s}(t)$ and the impulse-modulation model of sampling. Figure 2.6(a) is the sampled-data system which contains a discrete-time controller C_d , this is equivalent to what is shown in Figure 2.6(b) where the sampler is moved and the controller is now continuous-time, denoted by C_a . Now all the compartments in Figure 2.6(b) are continuous-time, except the sampled signal x before it is held by the ZOH. Next step is to replace the discretization by the impulse-modulation model as shown in Figure 2.6(c). Here the input of ZOH is denoted by $\hat{x}(t)$.

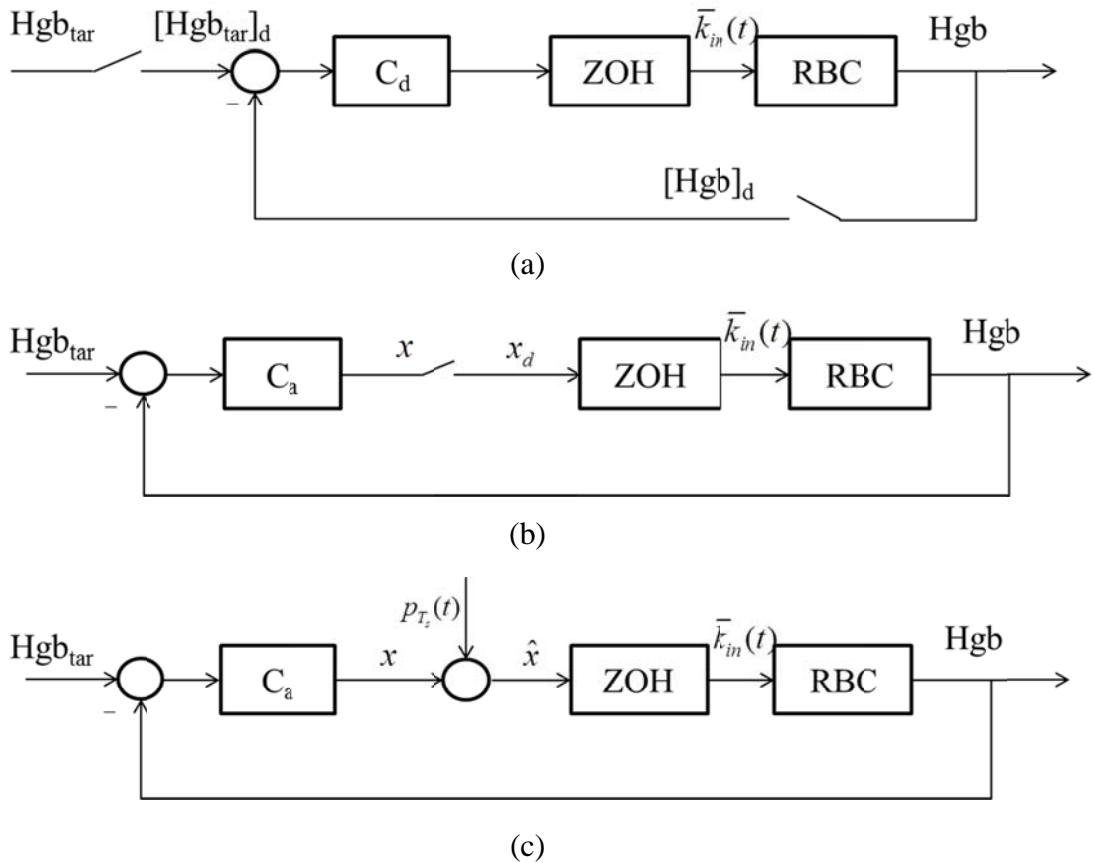


Figure 2.6: Sampling model

The sampled signal $\hat{x}(t)$ is

$$\begin{aligned}\hat{x}(t) &= x(t)p_{T_s}(t) \\ &= \sum_{n=0}^{\infty} x(t)\delta(t-nT_s),\end{aligned}$$

and its Fourier transform is

$$\begin{aligned}\hat{X}(j\omega) &= \frac{1}{2\pi} [X(j\omega) * P_{T_s}(j\omega)] \\ &= \frac{1}{T_s} \sum_{k=-\infty}^{\infty} X\left[j\left(\omega - \frac{2k\pi}{T_s}\right)\right].\end{aligned}$$

The Fourier transform of $\bar{k}_{in}(t)$ is

$$\bar{K}_{in}(j\omega) = \frac{1 - e^{-j\omega T_s}}{j\omega T_s} \sum_{k=-\infty}^{\infty} X\left[j\left(\omega - \frac{2k\pi}{T_s}\right)\right]$$

where the Fourier transform of the impulse response of the ZOH function is

$$\frac{1 - e^{-j\omega T_s}}{j\omega}.$$

The ZOH function may be represented by the transfer function $\frac{1 - e^{-sT_s}}{s}$ as shown

in Figure 2.7.

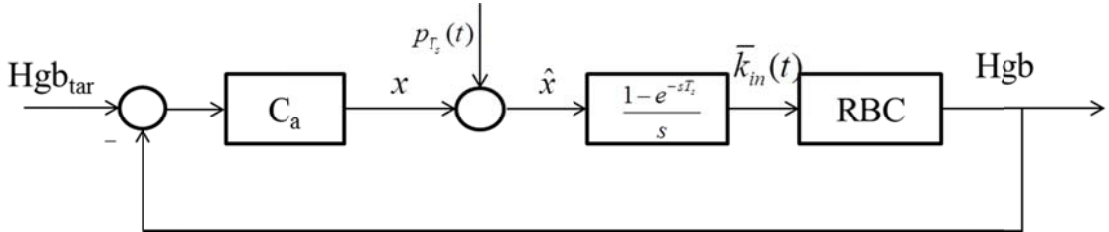


Figure 2.7: Impulse-modulation model for sampling

Equation $\hat{x}(t) = \sum_{n=0}^{\infty} x(t)\delta(t-nT_s)$ indicates that $\hat{X}(j\omega)$ is a periodic function in ω with period $\frac{2\pi}{T_s}$, comprised of a sum of frequency-shifted $X(j\omega)$, each with amplification factor $\frac{1}{T_s}$. As a result, $X(j\omega)$ can be theoretically recovered from

$\hat{X}(j\omega)$ if:

(i) $X(j\omega)$ itself is band-limited to $\left(0, \frac{\pi}{T_s}\right)$; said another way, the sampling frequency is appropriately chosen to avoid aliasing.

(ii) $\hat{X}(j\omega)$ is acted upon by an ideal low-pass filter with cut-off frequency of $\frac{\pi}{T_s}$.

In practice both of these conditions are simultaneously met when the complementary sensitivity function $T(s)$ of the AMCS is low-pass with a cut-off frequency less than $\frac{\pi}{T_s}$. Figure 2.8 illustrates this when it is assumed that the continuous-time AMP controller C_a results in such a closed-loop bandwidth, so now $\hat{X}(j\omega)$ is not a product as stated before but just a sum of the basic band signal and all the others.

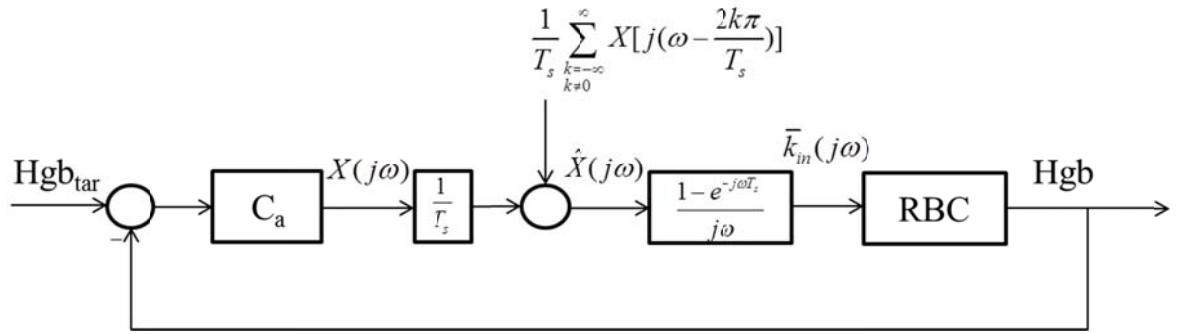


Figure 2.8: Impulse-modulation model for sampling (frequency domain)

From this block diagram,

$$X(j\omega) = T_s T(j\omega) [Hgb]_{tar}(j\omega) + T_s T(j\omega) \sum_{\substack{k=-\infty \\ k \neq 0}}^{\infty} X[j(\omega - \frac{2k\pi}{T_s})],$$

where $T(s)$ is the complementary sensitivity of this feedback system; i.e.,

$$T(s) = \frac{Q_a(s)}{1 + Q_a(s)},$$

where

$$Q_a(s) = H(s) \cdot \frac{1 - e^{-sT_s}}{sT_s} \cdot C_a(s).$$

When $T(s)$ is designed (via selection of C_a) so that it is a low-pass filter with cut-off frequency less than $\frac{\pi}{T_s}$, the Nyquist frequency, then

$$T(j\omega) \sum_{\substack{k=-\infty \\ k \neq 0}}^{\infty} X[j(\omega - \frac{2k\pi}{T_s})] \approx 0$$

$$X(j\omega) = T_s T(j\omega) Hgb_{tar}.$$

This is illustrated in the following block diagram representing a continuous-time approximation to the sampled-data model of AMCS.

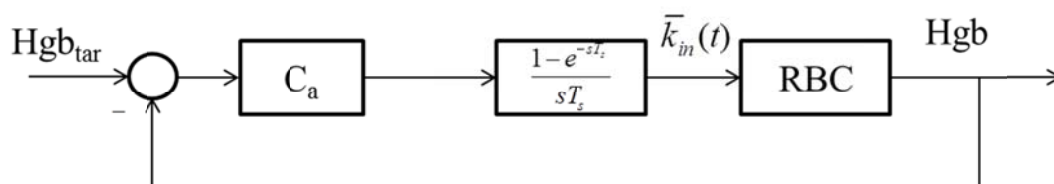


Figure 2.9: A simplified system

In this thesis, the continuous-time control system in Figure 2.10 will be the set-up upon which we will study robustness with respect to uncertainty in the RBC pool dynamics. Here $G_a(s) = \frac{1 - e^{-sT_s}}{sT_s}$. This setting is also useful for AMP design in that

the continuous-time controller C_a in Figure 2.10 leads directly to a protocol whose natural domain is discrete-time. We will now illustrate this using the Tustin transformation.

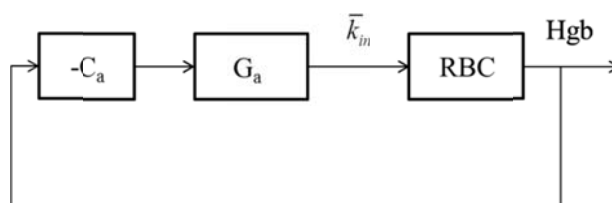


Figure 2.10: Simplified continuous-time system

Tustin's transformation is an algorithm mapping the s-plane to z-plane [13]. To illustrate, we take the AMP to be a PI controller with with proportional gain K_p and integral gain K_I ; the transfer function of which is given by

$$C_a(s) = K_p + \frac{K_I}{s}.$$

Tustin's algorithm uses the relationship

$$s = \frac{2}{T_s} \cdot \frac{z-1}{z+1},$$

so the approximate discrete-time controller has form

$$C_d(z) = C_a(s) \Big|_{s=\frac{2}{T_s} \frac{z-1}{z+1}} = K_p + K_I \cdot \frac{T_s(z+1)}{2(z-1)}.$$

In the following, we will approximate $G_a(s)$ by a rational function using a first-order Padé approximation:

$$G_a(s) = \frac{1 - e^{-sT_s}}{sT_s} = \frac{1}{1 + \frac{sT_s}{2}}.$$

We illustrate the continuous-time approximation in the next section.

2.3.3 Illustration

In the previous section, we introduced a continuous-time feedback system to approximate the sampled-data control system modeling an AMCS. In this section, we illustrate this approximation via simulation [14].

A simulation of such a sampled-data system is shown in Figure 2.11, with sampling time $T_s = 7$ days and RBC lifespan taken as a first-order gamma distribution with mean lifespan $\bar{\tau} = 100$ days. The AMP is a discrete-time PI controller with $K_p = 0.005$, $K_I = 0.0001$; i.e.,

$$C_d(z) = 0.005 + 0.00035 \frac{z+1}{z-1}.$$

The target value for Hgb is set to 11.25 g/dL, and the sampler is naturally embedded in the front-end of Simulink's discrete-time controller block.

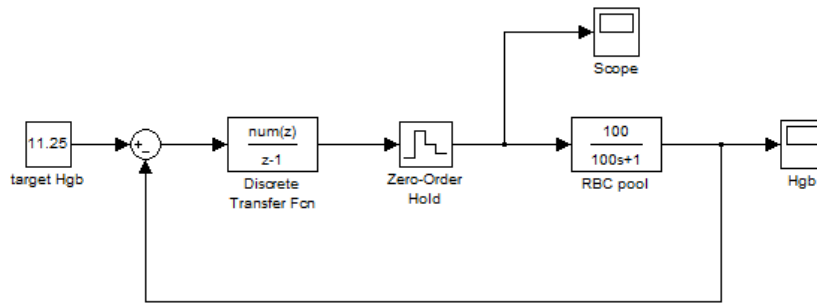


Figure 2.11: Simulink simulation for simplified sampled-data system

Figure 2.12 shows the simulation of the simplified continuous-time system, so applying the Tustin's transformation gives

$$C_a(s) = 0.005 + \frac{0.0001}{s},$$

and $G_a(s) = \frac{2}{7s+2}$ models the effect of both the sampler and the zero-order hold.

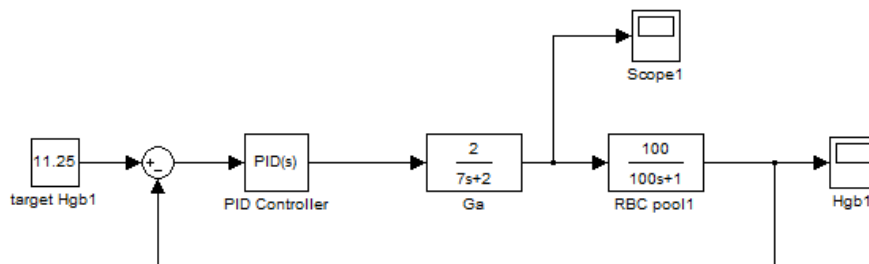
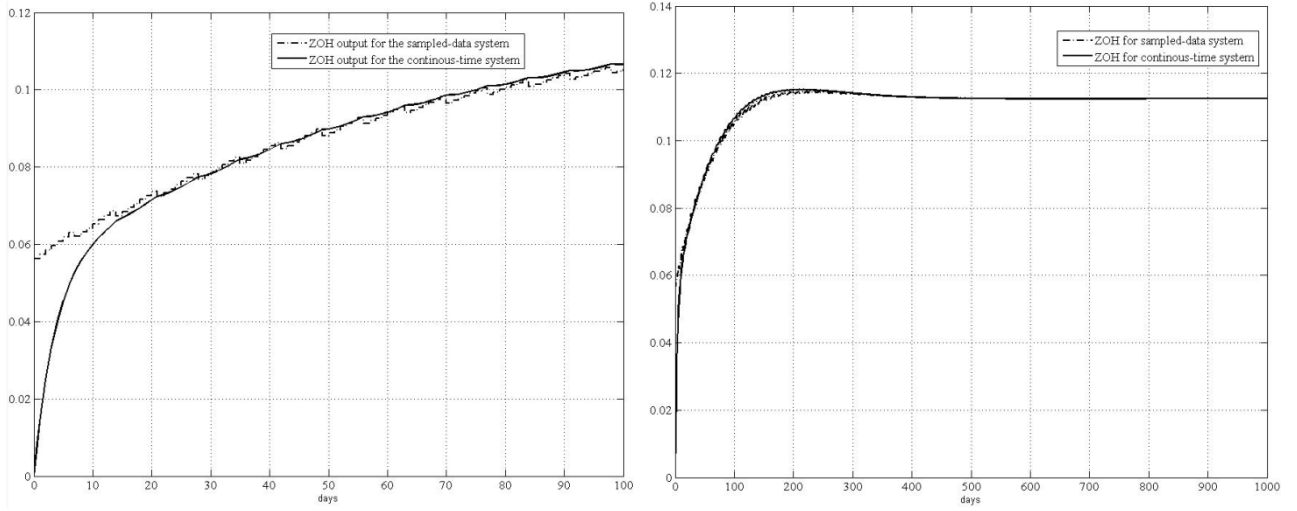


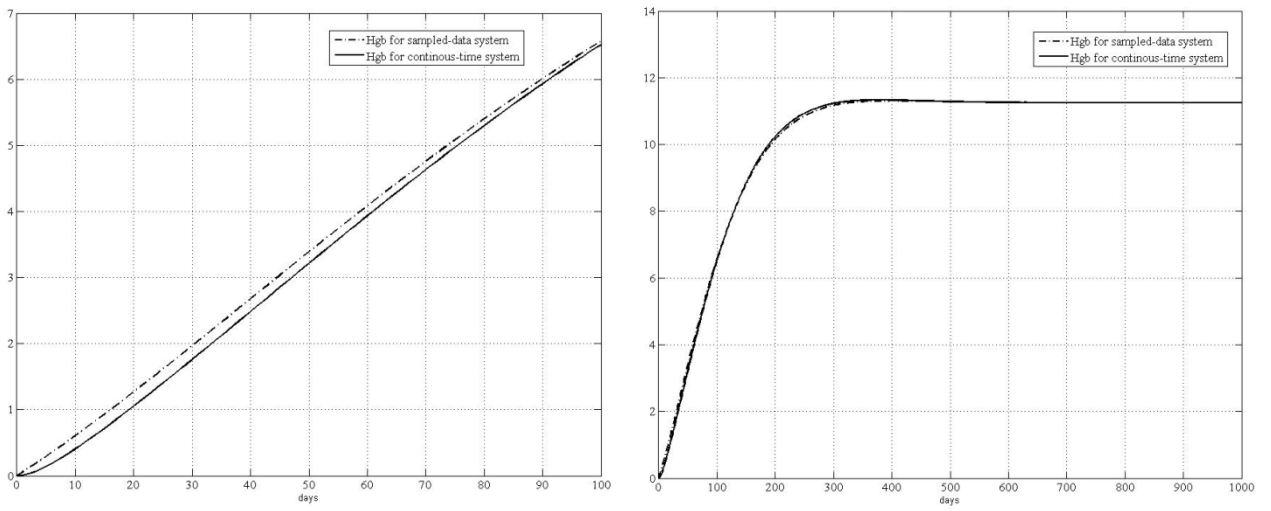
Figure 2.12: Simulation for approximated continuous-time system

Difference between the ZOH outputs of the two system is shown in Figure 2.13(a) for both short time (100 days) and longer time (1000 days), and in Figure 2.13(b) we show the comparison of outputs Hgb for both systems, in the same time scale as in (a). Since this is a simplified model, the assumption that Hgb starts at zero is applied. This is not true for a real system; however, this assumption is made to simplify the study.

There is not much difference between the outputs of the two systems, especially when in a longer time scale – consider the long lifespan of RBCs which is over 100 days. As a result, the approximation provided in previous section is reasonable.



(a)



(b)

Figure 2.13: Comparison of two systems

CHAPTER 3

UNCERTAINTY IN RBC POOL DYNAMICS (TIME-INVARIANT CASE)

In this chapter, we consider the time-invariant case of uncertainty in models for the RBC pool dynamics. The time-invariant modeling of RBC lifespan uncertainty takes into account the variability of the lifespan distribution from individual-to-individual. Several examples of lifespan distributions found in literature are reviewed, and we will look at some lifespan properties. By proposing the time-invariant uncertainty model, we first introduce a nominal system and look into multiplicative perturbation. Next, the robust stability of the system is discussed, where we propose a conjecture of the multiplicative error bound. Finally, the result of robustness is shown, as well as its implication on control design.

In Chapter 1, we modeled the RBC pool as a compartmental model, the input of which is the rate of newly-formed RBCs $\bar{k}_{in}(t)$ and output is the rate of eliminated RBCs $k_{out}(t)$. The hemoglobin pool content is determined by their difference as described by

$$\dot{Hgb}(t) = \bar{k}_{in}(t) - k_{out}(t)$$

where the elimination rate satisfies

$$k_{out}(t) = \int_0^t \bar{k}_{in}(t-\tau)l(\tau, t-\tau)d\tau$$

here $l(t, \tau)$ is the lifespan distribution. In the time-invariant case $l(t, \tau) \equiv l(\tau)$, the elimination rate becomes a convolution

$$k_{out}(t) = \int_0^t \bar{k}_{in}(t-\tau)l(\tau)d\tau \triangleq (\bar{k}_{in} * l)(t).$$

Here we rewrite the RBC pool dynamics showing the dependence on lifespan distribution explicitly

$$\dot{Hgb}(t) = \bar{k}_{in}(t) - (\bar{k}_{in} * l)(t).$$

3.1 Lifespan distributions

RBC lifespan uncertainty and its impact on AMCS is the focus of the thesis. In the time-invariant case, lifespan uncertainty can be interpreted as the variability of lifespan distribution from individual-to-individual.

We assume that each individual possesses a fixed, time-invariant RBC lifespan, but that these lifespans can differ from individual to individual.

3.1.1 Properties of lifespan distribution

We have computed the transfer function of the RBC pool in Chapter 1, which is

$$H(s) \triangleq \frac{\mathcal{L}\{Hgb(t)\}}{\mathcal{L}\{\bar{k}_m(t)\}} = \frac{1-L(s)}{s}$$

where $L(s)$ is the Laplace transform of the lifespan distribution $l(\tau)$. It is clear that the properties of the lifespan distribution function are essential in analyzing the dynamics of $H(s)$. Generally speaking, RBC lifespan is defined as a probability density function (pdf) [15]. Here, several properties of such pdf $l(\tau)$ are listed.

First of all, the lifespan distribution is non-negative; i.e.,

$$l(\tau) = \begin{cases} \geq 0, & \tau \geq 0 \\ 0, & \tau < 0 \end{cases}$$

where the lifespan $\tau \geq 0$ is the random variable. For each cell, the birth-time is assumed to be at time $t \geq 0$. Also, the lifespan should not be negative by definition.

Second, $l(\tau)$ satisfies:

$$\int_0^{\infty} l(\tau) d\tau = 1.$$

Third, mean RBC lifespan of a healthy individual is about 120 days [16], while that for a CKD patient may be less than 100 days. By definition the mean lifespan is:

$$\int_0^{\infty} \tau l(\tau) d\tau = \bar{\tau}.$$

3.1.2 Examples of lifespan distributions

Several RBC lifespan distribution functions have been proposed in the literature, including the gamma distribution [17], the Weibull [18] and the lognormal [6]. A summary is provided in [19]. Analysis shows that the gamma distribution and Weibull distributions can be good choices in modeling RBC lifespans; see [15].

The gamma distribution is defined as:

$$l_{k,\theta}(\tau) = \frac{1}{\theta^k} \frac{1}{\Gamma(k)} \tau^{k-1} e^{-\frac{\tau}{\theta}}$$

where τ is the lifespan, k and θ are positive constants. The mean and standard deviation for the gamma distribution are given by

$$\bar{\tau} = k\theta$$

and

$$\sigma = k\theta^2$$

respectively. This distribution has been used to describe the time taken for a cell to pass through k compartments (for example phases of the cell cycle), where the time spent in each compartment is exponentially distributed with the same parameter θ ; see [17]. To the mean lifespan $\bar{\tau}$, we re-parameterize the gamma distribution in terms of k and $\bar{\tau}$:

$$l_{k,\bar{\tau}}(\tau) = \frac{k^k}{\bar{\tau}^k} \frac{1}{\Gamma(k)} \tau^{k-1} e^{-\frac{k\tau}{\bar{\tau}}}$$

The Laplace transform of this parameterization of the gamma distribution is then

$$L(s) = \frac{1}{\left(\frac{s\bar{\tau}}{k} + 1\right)^k}$$

The Weibull function was introduced in the context of RBC lifespan in [18] and is given by

$$\frac{k}{\lambda} \left(\frac{\tau}{\lambda}\right)^{k-1} e^{-\left(\frac{\tau}{\lambda}\right)^k}$$

The two parameters are k and λ , and the mean value is given by

$$\bar{\tau} = \lambda \Gamma\left(1 + \frac{1}{k}\right).$$

In [18] Weibull distributions were used to model RBC lifespan values in humans; and done so with a mean lifespan of 120 days and a standard derivation of 15 days. Bebbington et al. [21] proposed a mixture of two modified Weibull distributions. They used two survival function to modify Weibull distributions, namely, $S_1(t)$ and $S_2(t)$, and used the mixture model

$$S(t) = pS_1(t) + (1-p)S_2(t)$$

with $p \in [0,1]$ mixing parameter.

The lognormal distribution was used to describe the p.d.f. for the reticulocyte lifespan in [6] with two parameters, σ and m , and function given by

$$\frac{1}{\sigma\tau\sqrt{2\pi}} e^{-\frac{(\ln\tau-m)^2}{2\sigma^2}}$$

with mean value

$$\bar{\tau} = e^{m + \frac{\sigma^2}{2}}.$$

In this thesis, we will focus on the family of gamma distribution for several reasons. First, it has been proved successful in approximating RBC lifespan via clinical data [15]. Second, the gamma distribution has rational Laplace transform. This is useful in applying feedback control theory, which is described by ordinary time-invariant finite-dimensional differential equation. Third, the two parameters, $\bar{\tau}$ and k , can directly relate to the physiology: $\bar{\tau}$ representing mean RBC lifespan and k the number of RBC developmental compartments. Also, the gamma distribution is widely used in the literatures [6, 15, 19, 20].

3.2 Time-invariant uncertainty model and robustness

The time-invariant case of RBC lifespan uncertainty assumes a fixed mean lifespan $\bar{\tau}$ and uncertain order k . In other words, we consider AMCS robustness to the order of lifespan gamma distribution; said another way, we consider a model where patients' RBC lifespan distributions are described by a gamma lifespan distribution with the

same mean RBC lifespan, but where the order k may differ from patient to patient. The model of uncertainty requires a so-called nominal lifespan, and for simplicity, a first-order ($k = 1$) gamma distribution is chosen. The next step is then to construct a model for perturbations to the nominal and derive robust stability conditions for the AMCS.

The main problem that we tackle for the remainder of this chapter is to build an uncertainty model, due to our lack of knowledge of this order parameter k . Such model of uncertainty can then be used to design an AMCS which performs robustly for all k .

3.2.1 Multiplicative error model

In feedback control design, a model of the physical system to be controlled is necessary. However, the model will never be a perfect description of the physical system. It is thus important to take the error [22] model and the physical system into account. In order to achieve this, an uncertainty model consisting of two components: a *nominal system*; and a set of perturbed systems that together are used to model the effects of system uncertainty [23]. The set consisting of this nominal model and perturbation is called the admissible perturbation model.

For feedback control system design, it is useful to describe the difference, or the system error between the nominal model and all the admissible perturbed models, and to bound this error. Several error models are common, such as the multiplicative and additive error models. We will use a multiplicative error model as shown in Figure 3.1

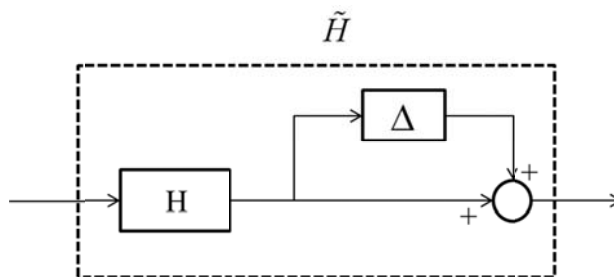


Figure 3.1: Perturbed model with multiplicative error

where H denotes the nominal transfer function of the RBC pool dynamic, \tilde{H} a perturbed transfer function, and Δ the associated multiplicative error defined by

$$\Delta(s) \triangleq \frac{\tilde{H}(s)}{H(s)} - 1.$$

3.2.2 Robust stability

Now we consider the AMCS and begin analysis of this feedback loop's performance over all admissible perturbed RBC dynamic \tilde{H} . We say that an AMP robustly stabilizes an AMCS if the AMCS is stable for every admissible perturbed RBC pool dynamic with transfer function \tilde{H} . Likewise, the AMCS is then said to be robustly stable.

Now we consider the details describing an admissible perturbed RBC dynamic. Given a time-invariant RBC lifespan pdf $l(\tau)$, it was shown in Section 1.3 that

$$\dot{Hgb}(t) = \bar{k}_in(t) - (\bar{k}_in * l)(t).$$

Taking the Laplace transform of both sides gives

$$H(s) \triangleq \frac{Hgb(s)}{K_in(s)} = \frac{1 - L(s)}{s}$$

where $Hgb(s)$, $k_in(s)$ and $L(s)$ denote the Laplace transforms of $Hgb(t)$, $\bar{k}_in(t)$ and $l(\tau)$ respectively. Suppose $l(\tau)$ is our best estimate of lifespan distribution for a patient population, and is referred to as the *nominal distribution*. By analogy $H(s)$ is called the nominal RBC dynamic, or nominal transfer function. Now, consider another plausible lifespan distribution for the population $\tilde{l}(\tau)$ and its corresponding RBC dynamic $\tilde{H}(s)$ the perturbed transfer function. One can then form the feedback control system as in Figure 2.10 where

$$\tilde{H}(s) = H(s)[1 + \Delta(s)],$$

with the multiplicative error

$$\Delta(s) \triangleq \frac{\tilde{H}(s)}{H(s)} - 1,$$

see Figure 3.2.

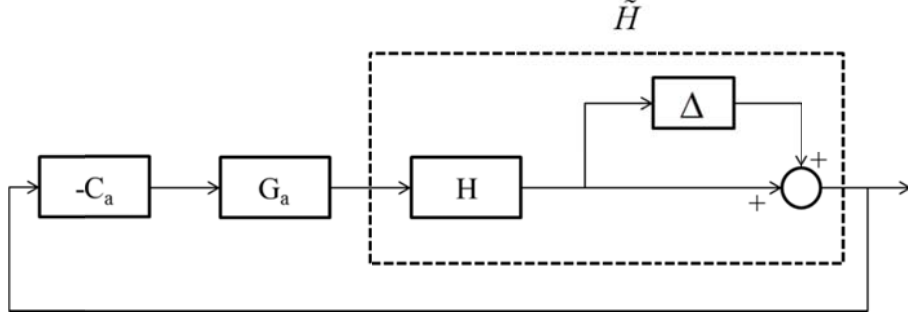


Figure 3.2: AMCS with perturbed RBC pool dynamic

The question for anemia management with respect to this setup is the following: Suppose the controller C stabilizes the feedback control system when the RBC dynamics is described by the nominal transfer function $H(s)$. Then, under what conditions does this same controller C stabilize the feedback loop when the RBC dynamics is the perturbed function $\tilde{H}(s)$? Said another way, when does an AMP, designed for stable Hgb regulation for patients with nominal lifespan distribution $l(\tau)$, also stabilize patients having the RBC lifespan distribution $\tilde{l}(\tau)$? This is a standard problem in robust control (for example see [22]), and to answer it we require $H(s)$ and $\tilde{H}(s)$ to share the same unstable poles¹, and require a stable transfer function W , referred to as a *multiplicative error bound*, such that

$$\left| \frac{\tilde{H}(j\omega)}{H(j\omega)} - 1 \right| \leq |W(j\omega)|, \quad \forall \omega \geq 0.$$

Let $T(s)$ denote the nominal complementary sensitivity function

$$T(s) = \frac{C_a G_a H(s)}{1 + C_a G_a H(s)}$$

and suppose C stabilizes the nominal feedback system; i.e., $T(s)$ is stable. Then, the perturbed complementary sensitivity function

$$\tilde{T}(s) \triangleq \frac{C_a G_a \tilde{H}(s)}{1 + C_a G_a \tilde{H}(s)}$$

is also stable if

$$\sup_{\omega} |TW(j\omega)| < 1, \quad \forall \omega \geq 0.$$

¹ This is a generally-stated requirement, and one that is satisfied for the RBC transfer functions considered here.

Now, we specialize the above general to the case of gamma distribution. Given a mean lifespan $\bar{\tau}$ and order k , consider the corresponding gamma lifespan distribution. Suppose $H_1(s)$ is taken as the nominal RBC dynamic and that there exists a stable transfer function W such that for each k ,

$$\left| \frac{H_k(j\omega)}{H_1(j\omega)} - 1 \right| \leq |W(j\omega)|, \quad \forall \omega \geq 0.$$

Note that W is a valid multiplicative error bound for all perturbed RBC transfer functions H_k . Suppose the nominal closed-loop is stable; i.e.,

$$T_1(s) \triangleq \frac{C_a G_a H_1(s)}{1 + C_a G_a H_1(s)}$$

is stable. Then, given any k , it follows from the previous that C stabilizes the perturbed feedback system; that is,

$$T_k(s) \triangleq \frac{C_a G_a H_k(s)}{1 + C_a G_a H_k(s)}$$

is stable, provided that

$$\sup_{\omega} |T_1 W(j\omega)| < 1, \quad \forall \omega \geq 0.$$

The existence of such multiplicative error bound W - one that bounds for all perturbed transfer functions H_k - is critical for the preceding result to be practically useful.

3.3 Error bounds

In this subsection we provide some useful bounds on the multiplicative error

$\left| \frac{H_k(j\omega)}{H_1(j\omega)} - 1 \right|$. The first bound is looser than the second; however, whereas the former

is a provable bound, the latter is only conjectural to be the tightest bound.

3.3.1 A multiplicative error bound

Given mean lifespan $\bar{\tau}$, define

$$\gamma(\omega) = \begin{cases} \frac{\sqrt{30}}{9} \cdot \omega \bar{\tau}; & 0 \leq \omega \bar{\tau} < 1 \\ 1 + \frac{2}{\omega \bar{\tau}}; & \omega \bar{\tau} \geq 1 \end{cases}$$

and let $\bar{W}(s)$ be a stable transfer function such that $\gamma(\omega) \leq |\bar{W}(j\omega)|$ for all $\omega \geq 0$.

Indeed, transfer function of the form $\bar{W}(s) = \frac{k_1 s}{s + k_2}$ will suffice for some $k_1, k_2 > 0$.

We now prove that $\bar{W}(j\omega)$ is a multiplicative error bound, and before doing so, we recall from the previous section, that

$$H_1(j\omega) = \frac{1 - L_1(j\omega)}{j\omega}; \quad H_k(j\omega) = \frac{1 - L_k(j\omega)}{j\omega}$$

where $L_1(s)$ and $L_k(s)$ are the Laplace transforms for $l_{\bar{\tau},1}(\tau)$ and $l_{\bar{\tau},k}(\tau)$ respectively, and where k is an integer greater than zero.

Theorem 3.1 (see proof in appendix A): Let $\bar{\tau} > 0$ and k a positive integer be given. Then,

$$\left| \frac{H_k(j\omega)}{H_1(j\omega)} - 1 \right| \leq \gamma(\omega) \leq \bar{W}(j\omega)$$

for all $\omega \geq 0$. Hence, $\bar{W}(j\omega)$ is multiplicative error bound; in Figure 3.3, we verify the bound $\gamma(\omega)$ for $\bar{\tau} = 100$ days and $k = 2, 3, \dots, 100$.

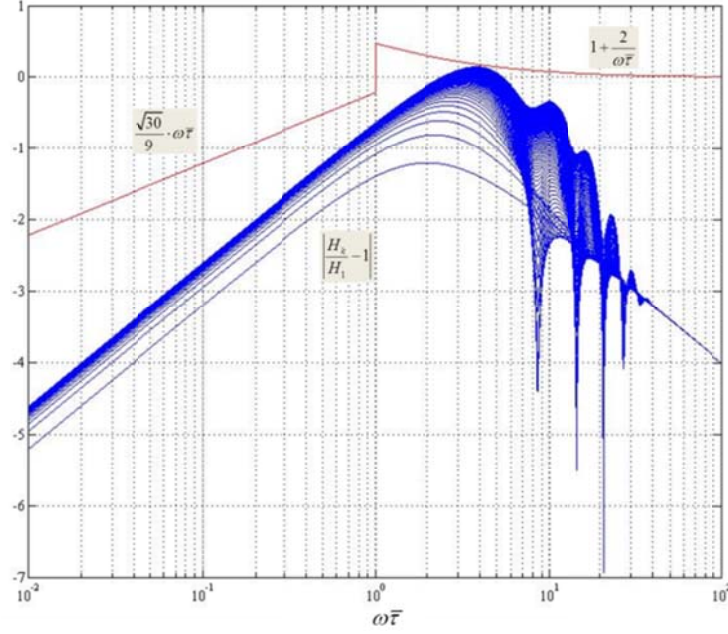


Figure 3.3: Verification of Theorem 3.1 for $\bar{\tau} = 100$ and $k = 2, 3, \dots, 100$

3.3.2 Conjectured tighter bound

We now conjecture a tighter error bound.

Conjecture: Given mean lifespan $\bar{\tau}$, let

$$\hat{W}(s) \triangleq \frac{1 - (1 + s\bar{\tau})e^{-s\bar{\tau}}}{s\bar{\tau}}.$$

Then given k ,

$$\left| \frac{H_k(j\omega)}{H_1(j\omega)} - 1 \right| \leq |\hat{W}(j\omega)| \leq \gamma(\omega), \quad \forall \omega \geq 0.$$

Furthermore,

$$\left| \frac{e^{-j\omega\bar{\tau}}}{H_1(j\omega)} - 1 \right| = |\hat{W}(j\omega)|, \quad \forall \omega \geq 0,$$

showing that the error bound is achieved for the lifespan distribution $l(\tau) = \delta(\tau - \bar{\tau})$.

Figure 3.4 verifies the conjecture for $\bar{\tau} = 100$ and $k = 2, 3, \dots, 10000$.

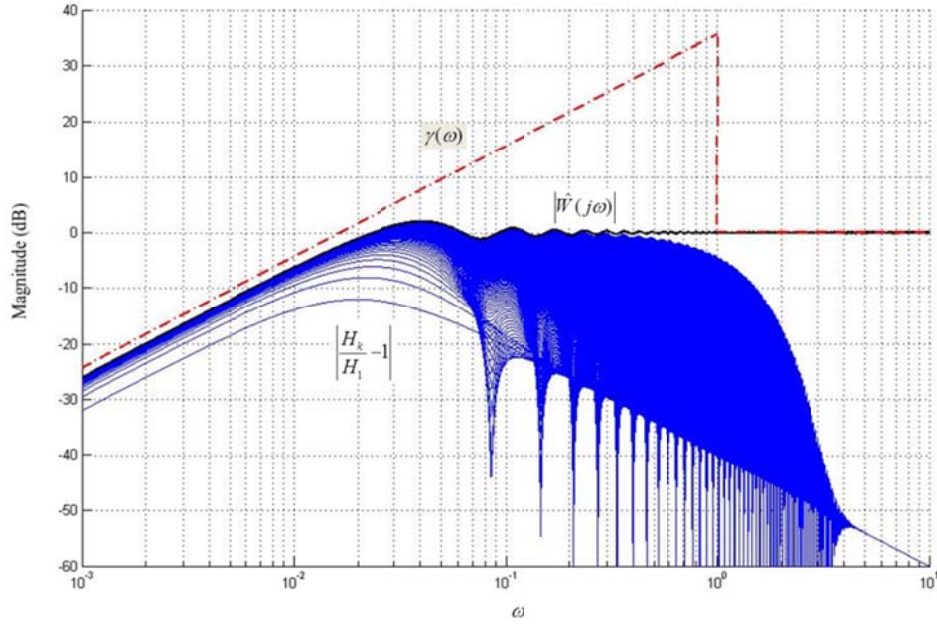


Figure 3.4: Matlab example of the conjecture for $k = 2, 3, \dots, 10000$

3.4 Robust stability

In this section, we apply the error bounds determined in the previous section to the design of robustly stabilizing AMPs. For the error bound \hat{W} , the condition for robust

stability is $\sup_{\omega \geq 0} |\overline{W}T_1| < 1$. In Figure 3.5, we provide a bode plot $\left| \frac{1}{\hat{W}} \right|$ and $|T_1|$ when

$$K_p = 0.005; \quad K_I = 0.0001; \quad T_s = 7; \quad \bar{\tau} = 100, \quad \text{and} \quad C_a(s) = K_p + \frac{K_I}{s} = 0.005 + \frac{0.0001}{s};$$

$$G_a(s) = \frac{\frac{2}{T_s}}{s + \frac{2}{T_s}} = \frac{2}{7s + 2}; \quad H_1(s) = \frac{1 - L_1(s)}{s} = \frac{100}{100s + 1}.$$

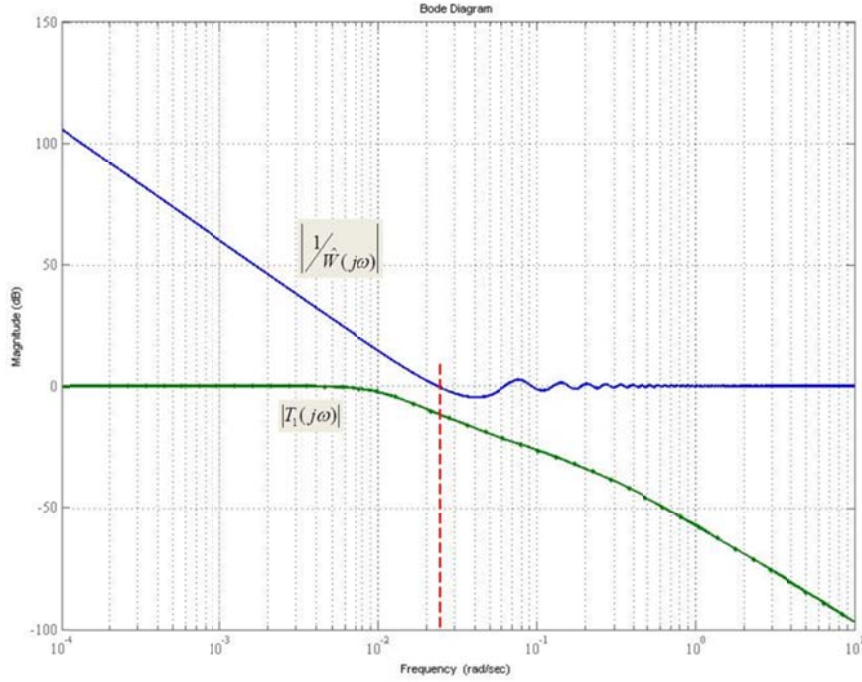


Figure 3.5: Robust stability for LTI case

It is clear from Figure 3.5 that $\sup_{\omega \geq 0} |\hat{W}T_1| < 1$ and hence that the controller $C_a(s)$ robustly stabilizes this AMCS. From Figure 3.5, we also can notice that the error bound \hat{W} places a bandwidth² constraint on the closed-loop transfer function of about 0.025 rad/day. In designing a PI controller for this system, if the bandwidth goes beyond the constraint, it is possible that the stability criterion will be violated.

The robust stability criterion $\sup |\hat{W}T| < 1$ is useful in AMP design. With $Q(s)$ denoting the compensated open-loop transfer function

$$Q(s) \triangleq C_a \cdot G_a \cdot H_1(s),$$

then for those frequencies ω such that $|P(j\omega)| \ll 1$, it follows that

$$|T_1(j\omega)| = \left| \frac{Q(j\omega)}{1 + Q(j\omega)} \right| \approx |Q(j\omega)|.$$

Consequently for these sets of frequencies ω , the robust stability condition is ensured if

² Roughly speaking the bandwidth is the corner frequency of the low-pass filter characteristic of $|T(j\omega)|$.

$$|Q(j\omega)| < \left| \frac{1}{\hat{W}(j\omega)} \right|.$$

This inequality provides a design guideline for $C_a(s)$ in high frequency ranges. In the next figure, we use the previous data and show that Bode plots for $|Q(j\omega)|$ and $\left| \frac{1}{\hat{W}(j\omega)} \right|$ to confirm that this particular AMP design satisfies $|Q(j\omega)| < \left| \frac{1}{\hat{W}(j\omega)} \right|$.

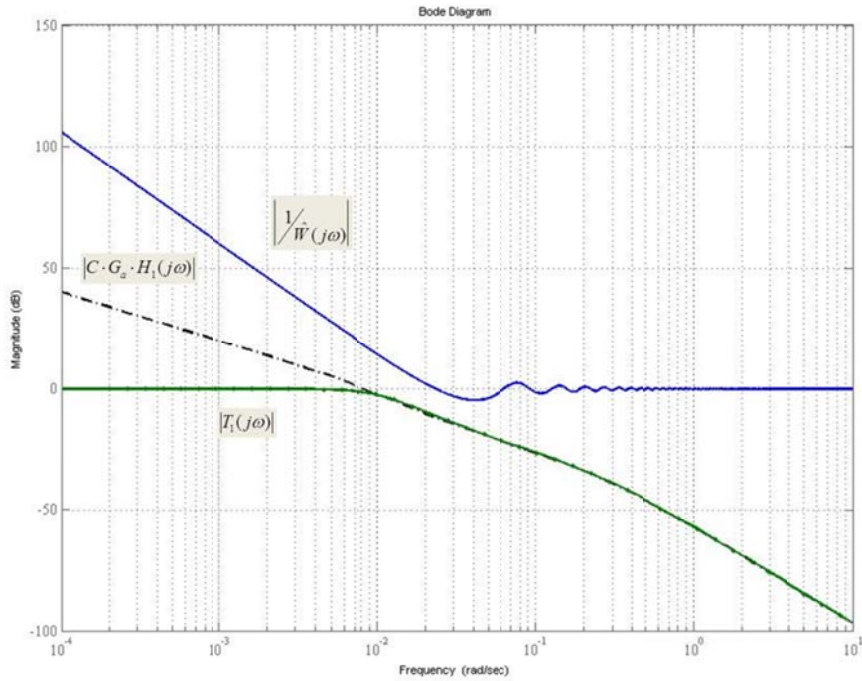


Figure 3.6: Implication on control design

3.5 Robust performance

Now we consider the notion of robust performance which together with robust stability includes a performance constraint on all perturbed models in \tilde{H} .

Nominal Performance: First, we introduce the notion of nominal performance. Suppose the target Hgb level is Hgb_{tar} . The tracking error between Hgb_{tar} and measured Hgb is the tracking error e which can be expressed in the frequency domain by

$$E(j\omega) = S(j\omega)Hgb_{tar}(j\omega)$$

where S is the sensitivity function of the feedback loop and given by

$$S(s) \triangleq \frac{1}{1 + C_a G_a H(s)}.$$

In practice, $Hgb_{tar} \equiv \text{constant}$, say $Hgb_{tar} \equiv h_0$ so that

$$Hgb_{tar}(j\omega) = \frac{h_0}{j\omega}$$

and from the above

$$|E(j\omega)| = |S(j\omega)| \cdot \frac{h_0}{\omega}.$$

Suppose we impose the tracking error bound ε_e so that

$$|E(j\omega)| \leq \varepsilon_e, \quad \forall \omega > 0.$$

This error bound ε_e precludes $e(t)$ having any persistent signal components and imposes that $S(0) = 0$. Also, it places a bound on the closed-loop bandwidth.

Suppose the bandwidth is ω_{BW} ; i.e.,

$$|S(j\omega)| = \left| \frac{E(j\omega)}{Hgb_{tar}(j\omega)} \right| \leq \left| \frac{j\omega\varepsilon_e}{h_0} \right| < 1, \quad 0 \leq \omega \leq \omega_{BW}.$$

It then follows that

$$\omega_{BW} < \frac{h_0}{\varepsilon_e}.$$

Notice that the closed-loop time constant is approximately $\frac{1}{\omega_{BW}}$. Thus smaller ε_e 's

leads to faster-responding AMCS. Now, let $W_p(j\omega) \triangleq \frac{h_0}{\varepsilon_e \omega}$, then $\sup_{\omega > 0} |E(j\omega)| \leq \varepsilon_e$,

provided that $\sup_{\omega > 0} |W_p S(j\omega)| < 1$.

In summary, nominal Hgb tracking performance can be modeled by the frequency-domain constraint

$$\sup_{\omega} |W_p S(j\omega)| < 1$$

where W_p models Hgb target-tracking performance and we set $h_0 = 11.25, \varepsilon_e = 2000$. Figure 3.7 gives a graphical illustration of this nominal performance constraint, where we have the same parameters as in previous section; i.e.,

$$C_a(s) = 0.005 + \frac{0.0001}{s}, G_a(s) = \frac{2}{7s+2}, H_1(s) = \frac{100}{100s+1}.$$

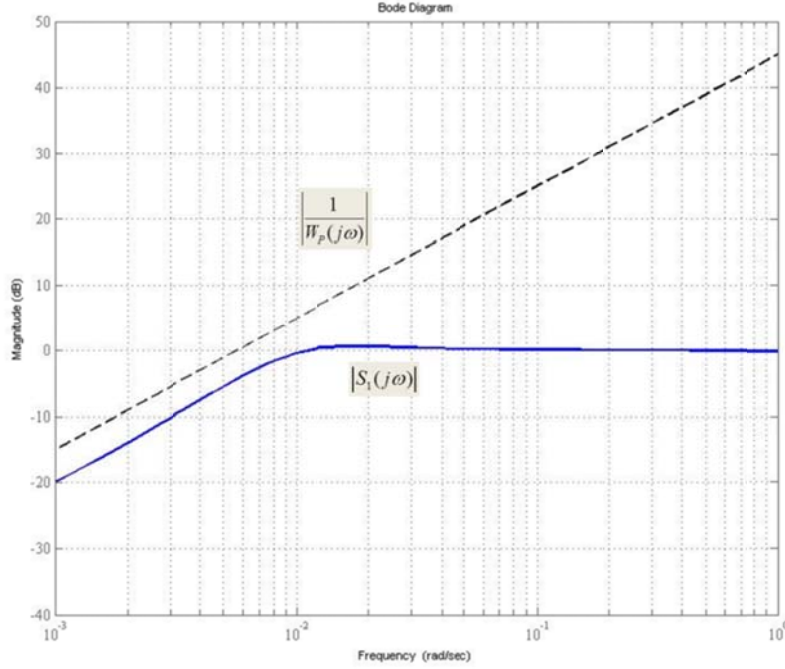


Figure 3.7: Nominal performance of AMP

Notice that this particular nominal performance constraint $\left| \frac{1}{W_p(j\omega)} \right|$ requires $S(0) = 0$ and for $C_a(s)$ to contain an integrator, which it does.

Robust Performance: Let $S_k(s)$ denotes the sensitivity function for the feedback system in Figure 3.2, our model of an AMCS, when the perturbed RBC dynamic has transfer function $H_k(s)$. With the performance weight W_p as given previously, we say that an AMP $C_a(s)$ achieves robust performance if

$$\sup_{\omega} |W_p S_k(j\omega)| < 1$$

for all gamma distribution orders k . Such an AMP insures closed-loop stability and Hgb target tracking performance for all $H_k(s)$. From [22], the preceding condition is equivalent to

$$\sup_{\omega} \left[|W_p S_1| + |\hat{W} T_1| \right] < 1$$

whose significance lies in the fact that robust performance can be quantified solely in terms of the nominal feedback system's sensitivity function S_1 and complementary sensitivity transfer function T_1 . In the next figure we plot $|W_p S_1(j\omega)| + |\hat{W} T_1(j\omega)|$ for the same design parameters previously use.

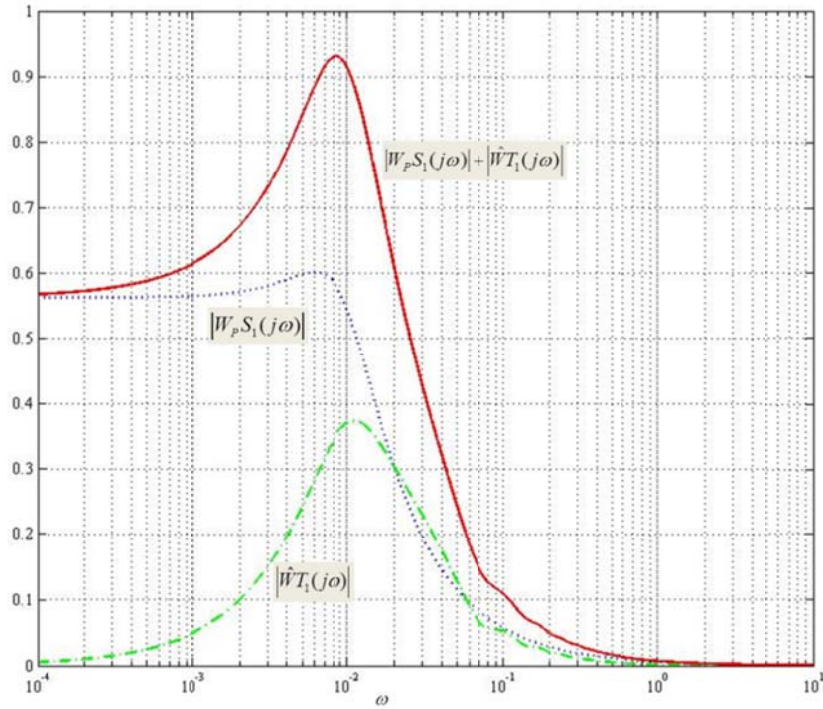


Figure 3.8: Robust performance for the time-invariant system

From Figure 3.8, we can see that the robust performance condition $\sup_{\omega} \left[|W_p S_1| + |\hat{W} T_1| \right] < 1$ is satisfied. This indicates that the system successfully achieves both robust stability and robust performance with the designed controller.

CHAPTER 4

UNCERTAINTY IN RBC POOL DYNAMICS (TIME-VARYING CASE)

In contrast to the time-invariant case considered in the previous chapter we now consider RBC lifespan distributions that can vary with time. In this chapter, we will introduce a RBC model to capture these time-variations and evaluate stability robustness of the AMCS by seeking a quadratic Lyapunov function. As in the time-invariant case, we will also consider robust performance and use the dominant AMCS time constant as the performance measure.

4.1 Time-varying lifespan distributions

Chapter 3 considered a time-invariant model of the lifespan distribution which is fixed in time for an individual, but perhaps variable over the population. However, the RBC pool dynamics may be better modeled using a time-varying lifespan distribution to account for temporal variations in an individual's erythropoiesis processes; e.g., see [18, 24]. Here we assume a time-varying model where there exist a finite number of potential lifespan distributions, and where each newly-born RBC is endowed with a lifespan chosen from this collection.

Our time-varying model is as follows. For a given individual and at time t , the RBC lifespan distribution is arbitrarily chosen from a pre-determined finite set of N time-invariant distributions,

$$l(t, \tau) \in \{l_1(\tau), l_2(\tau), \dots, l_N(\tau)\}.$$

We assume that $l(t, \tau)$ is a measurable function of time.

As in the time-invariant lifespan model considered in Chapter 3, the family of gamma distributions considered is:

$$l_{k, \bar{\tau}}(\tau) = \frac{k^k}{\bar{\tau}^k} \frac{1}{\Gamma(k)} \tau^{k-1} e^{-\frac{k\tau}{\bar{\tau}}},$$

where the set of possible distributions is parameterized by mean lifespan $\bar{\tau}$ and gamma distribution order k ; i.e.,

$$l(t, \tau) \in \{l_{k_1, \bar{\tau}_1}(\tau), l_{k_2, \bar{\tau}_2}(\tau), \dots, l_{k_N, \bar{\tau}_N}(\tau)\}.$$

This model reflects the possibility that for an individual, every newly-born RBC is endowed with a lifespan chosen from a set of given time-invariant gamma distributions.

4.2 RBC dynamics for time-varying lifespan distributions

In the previous section, we introduced a time-varying lifespan model where lifespans are arbitrarily chosen from a given and fixed set of time-invariant gamma distributions. This model, given by $l(t, \tau) \in \{l_{k_1, \bar{\tau}_1}(\tau), l_{k_2, \bar{\tau}_2}(\tau), \dots, l_{k_N, \bar{\tau}_N}(\tau)\}$, can also be expressed as

$$l(t, \tau) = \sum_{i=1}^N \lambda_i(t) l_{k_i, \bar{\tau}_i}(\tau); \quad \lambda_i(t) \in \{0, 1\}; \quad \sum_{i=1}^N \lambda_i(t) \equiv 1,$$

where $\lambda_i(t)$ are measurable functions of time. From a technical viewpoint, this particular model of time-varying lifespan displays a separation between time t and the lifespan random variable τ in that $l(t, \tau)$ can be written as the product

$$l(t, \tau) = \begin{bmatrix} \lambda_1(t) & \lambda_2(t) & \dots & \lambda_N(t) \end{bmatrix} \begin{bmatrix} l_{k_1, \bar{\tau}_1}(\tau) \\ l_{k_2, \bar{\tau}_2}(\tau) \\ \vdots \\ l_{k_N, \bar{\tau}_N}(\tau) \end{bmatrix}$$

where each factor depends only on t or τ . This separation will allow us to decompose the time-varying convolution integral associated with the RBC pool dynamic

$$\int_0^t \bar{k}_{in}(\tau) l(\tau, t - \tau) d\tau$$

in terms of convolutions associated with the time-invariant lifespans

$$\int_0^t \bar{k}_{in}(\tau) l_{k_i, \bar{\tau}_i}(t - \tau) d\tau.$$

To see this property's use, we write, under the assumption $\sum_{i=1}^N \lambda_i(t) \equiv 1$:

$$\begin{aligned} \dot{Hgb}(t) &= \bar{k}_{in}(t) - \int_0^t \bar{k}_{in}(\tau) l(\tau, t - \tau) d\tau \\ &= \bar{k}_{in}(t) - \int_0^t \bar{k}_{in}(\tau) \sum_{i=1}^N \lambda_i(\tau) l_{k_i, \bar{\tau}_i}(\tau, t - \tau) d\tau \\ &= \sum_{i=1}^N \lambda_i(t) \bar{k}_{in}(t) - \sum_{i=1}^N \int_0^t \lambda_i(\tau) \bar{k}_{in}(\tau) l_{k_i, \bar{\tau}_i}(\tau, t - \tau) d\tau. \end{aligned}$$

This differential equation is illustrated in Figure 4.1. With this, the RBC pool can be considered as a collection of N sub-pools where the i -th sub-pool contains only RBCs with lifespans chosen from distribution $l_{k_i, \bar{\tau}_i}(\tau)$. The uncertain parameters $\lambda_i(t)$ then determine which sub-pool a newly-born RBC joins.

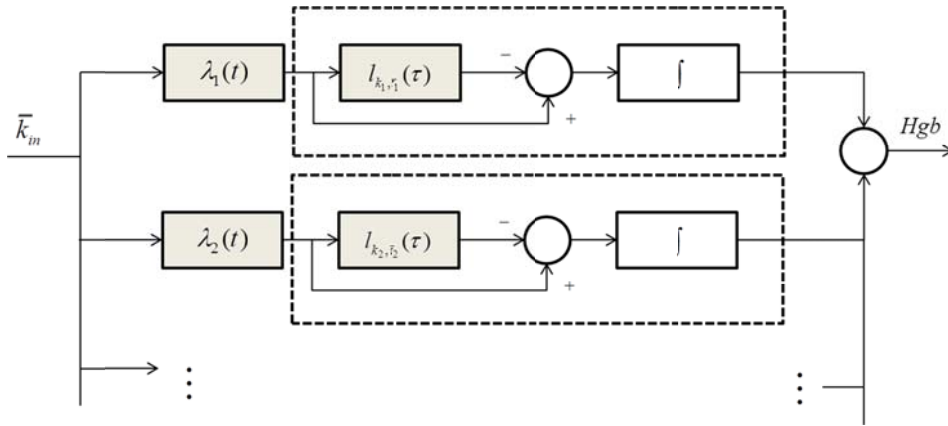


Figure 4.1: Time-varying RBC pool with sub-pools

In Figure 4.1, the boxed blocks represent the time-invariant sub-pools. The condition

$$\lambda_i(t) \in \{0, 1\}; \quad \sum_{i=1}^N \lambda_i(t) \equiv 1$$

means that at time t , a new RBC entering circulation becomes a member of only one sub-pool.

4.3 The AMCS

In this section we look at the differential equation describing the AMCS when the RBC lifespan is time-varying. The open-loop consists of three sub-systems: the PI

AMP C_a , the sampler and hold function G_a , and the RBC pool dynamic (RBC). We will write down the differential equation for each compartmental dynamic and then generate that for the closed-loop system.

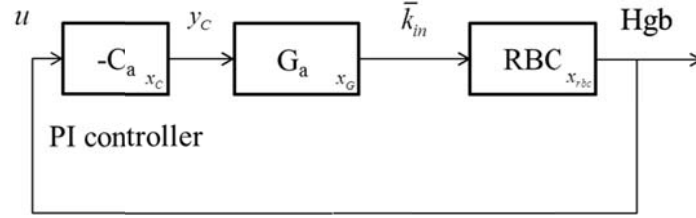


Figure 4.2: Simplified state-space model of AMP system

Figure 4.2 shows the AMCS block diagram annotated with system states $\{x_c, x_G, x_{rbc}\}$. Let $C_a(s)$ denotes the transfer function of a PI AMP, with proportional and integral parameters K_p and K_i respectively. The transfer function of the PI controller is

$$C_a(s) = K_p + \frac{K_i}{s},$$

and with the input of $-u$, it is described by the differential equation

$$\begin{aligned}\dot{x}_c &= -K_i u \\ y_c &= x_c - K_p u.\end{aligned}$$

The AMP's state space representation is then

$$[A_c, B_c, C_c, D_c] = [0, -K_i, 1, -K_p].$$

In Chapter 3, an approximation of sample and zero-order hold was given as

$$G_a(s) = \frac{\frac{2}{T_s}}{s + \frac{2}{T_s}}$$

and its differential equation is

$$\begin{aligned}\dot{x}_G &= -\frac{2}{T_s} x_G + \frac{2}{T_s} y_c \\ \bar{k}_{in} &= x_G\end{aligned}$$

with corresponding state space $[A_G, B_G, C_G, D_G] = \left[-\frac{2}{T_s}, \frac{2}{T_s}, 1, 0\right]$.

Let x_{rbc_i} and $[A_i, B_i, C_i]$ be the state and state representation for $l_{k_i, \bar{\tau}_i}(\tau)$ respectively. Now consider the case $N=2$, the differential equations for the two RBC sub-pools are

$$\begin{aligned}\dot{x}_{rbc1} &= A_1 x_{rbc1} + \lambda_1(t) B_1 \bar{k}_{in}; \\ Hgb_1 &= C_1 x_{rbc1}\end{aligned}$$

and

$$\begin{aligned}\dot{x}_{rbc2} &= A_2 x_{rbc2} + \lambda_2(t) B_2 \bar{k}_{in}; \\ Hgb_2 &= C_2 x_{rbc2}\end{aligned}$$

where $Hgb = Hgb_1 + Hgb_2$. Figure 4.3 illustrates the structure of the two sub-pools.

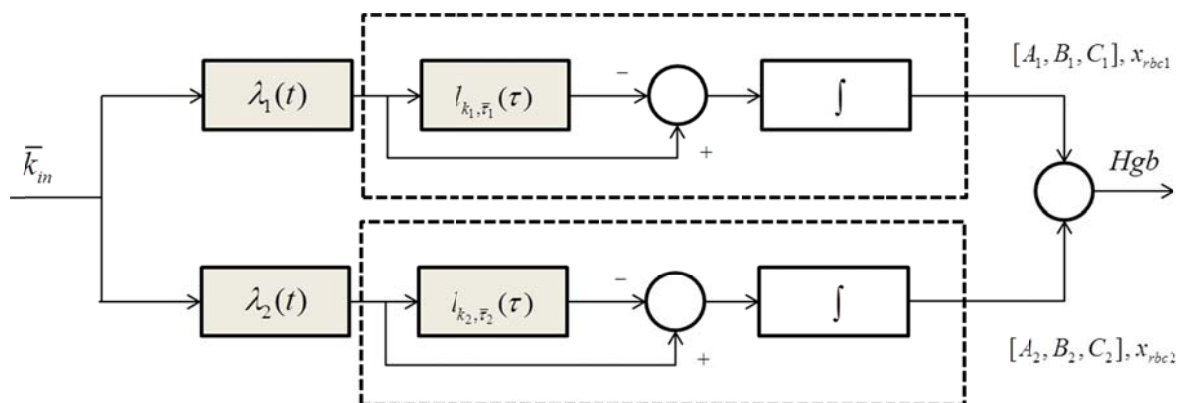


Figure 4.3: Time-varying model of RBC pool with two potential lifespans

The concatenation of states $[x_{rbc1}, x_{rbc2}]^T$ has differential equation

$$\begin{aligned}\begin{bmatrix} \dot{x}_{rbc1} \\ \dot{x}_{rbc2} \end{bmatrix} &= \begin{bmatrix} A_1 & 0 \\ 0 & A_2 \end{bmatrix} \begin{bmatrix} x_{rbc1} \\ x_{rbc2} \end{bmatrix} + \begin{bmatrix} \lambda_1(t) B_1 \\ \lambda_2(t) B_2 \end{bmatrix} \bar{k}_{in} \\ Hgb &= [C_1 \quad C_2] \begin{bmatrix} x_{rbc1} \\ x_{rbc2} \end{bmatrix}\end{aligned}$$

and for notational purposes we identify:

$$A_{rbc} = \begin{bmatrix} A_1 & 0 \\ 0 & A_2 \end{bmatrix}; \quad B_{rbc}(t) = \begin{bmatrix} \lambda_1(t) B_1 \\ \lambda_2(t) B_2 \end{bmatrix}; \quad C_{rbc} = [C_1 \quad C_2].$$

From Figure 4.2, the feedback equation is $u = Hgb$, so that the state space equation for the closed-loop system can be expressed as

$$\dot{x}_{cl} = \begin{bmatrix} \dot{x}_{rbc} \\ \dot{x}_G \\ \dot{x}_C \end{bmatrix} = \begin{bmatrix} A_{rbc} & B_{rbc}(t) & 0 \\ -\frac{2}{T} K_p C_{rbc} & -\frac{2}{T_s} & \frac{2}{T_s} \\ -K_I C_{rbc} & 0 & 0 \end{bmatrix} x_{cl}$$

where x_{cl} is the state of the closed-loop system.

Defining

$$A_{cl}(t) \triangleq \begin{bmatrix} A_{rbc} & B_{rbc}(t) & 0 \\ -\frac{2}{T} K_p C_{rbc} & -\frac{2}{T_s} & \frac{2}{T_s} \\ -K_I C_{rbc} & 0 & 0 \end{bmatrix}; \quad t \geq 0,$$

gives the state-space representation of the closed-loop system as

$$\dot{x}_{cl} = A_{cl}(t)x_{cl}; \quad t \geq 0.$$

For the case of $N = 2$, denote the corresponding closed-loop matrices A_{cl1} and A_{cl2} as

$$A_{cl1} \triangleq \begin{bmatrix} A_1 & 0 & B_1 & 0 \\ 0 & A_2 & 0 & 0 \\ -\frac{2}{T_s} K_p C_1 & -\frac{2}{T_s} K_p C_2 & -\frac{2}{T_s} & \frac{2}{T_s} \\ -K_I C_1 & -K_I C_2 & 0 & 0 \end{bmatrix};$$

$$A_{cl2} \triangleq \begin{bmatrix} A_1 & 0 & 0 & 0 \\ 0 & A_2 & B_2 & 0 \\ -\frac{2}{T_s} K_p C_1 & -\frac{2}{T_s} K_p C_2 & -\frac{2}{T_s} & \frac{2}{T_s} \\ -K_I C_1 & -K_I C_2 & 0 & 0 \end{bmatrix}.$$

These matrices correspond to A_{cl} when (λ_1, λ_2) is $(1, 0)$ and $(0, 1)$ respectively. Given these two matrices, we can express the closed-loop dynamics for $N = 2$ compactly as

$$\dot{x}_{cl} = A_{cl}(t)x_{cl}; \quad A_{cl}(t) \in \{A_{cl1}, A_{cl2}\}$$

which generalizes to the general case as

$$\dot{x}_{cl} = A_{cl}(t)x_{cl}; \quad A_{cl}(t) \in \{A_{cl1}, A_{cl2}, \dots, A_{clN}\}.$$

Since $\lambda_i(t)$ are measurable, then $A_{cl}(t)$ is also measurable.

4.4 Quadratic stability

First, we introduce the notion of exponential stability. The given time-varying system is

$$\dot{x}_{cl} = A_{cl}(t)x_{cl}; A_{cl}(t) \in \{A_{cl1}, A_{cl2}, \dots, A_{clN}\}; t \geq 0; x_{cl}(0) = x_{cl0}.$$

Since $A_{cl}(t)$ is measurable, then this differential equation has a solution almost everywhere in some interval $t \in [0, t_1]$; e.g., see [30]. Next, we will discuss the exponential stability of this differential equation. Exponential stability indicates that $\dot{x}_{cl} = A_{cl}(t)x_{cl}$ has a solution over all $t \in [0, \infty)$; e.g., see [31].

This differential equation is said to be exponentially stable (around $x_{cl0} = 0$) if there exist numbers $\alpha, \beta \geq 0$ such that

$$\|x_{cl}(t)\| \leq \beta \|x_{cl0}\| e^{-\alpha t}; \forall t \geq 0.$$

A plot of an exponentially stable system can be seen in Figure 4.4 where $\|x_{cl}(t)\|$ is bounded by $\beta \|x_{cl0}\| e^{-\alpha t}$.

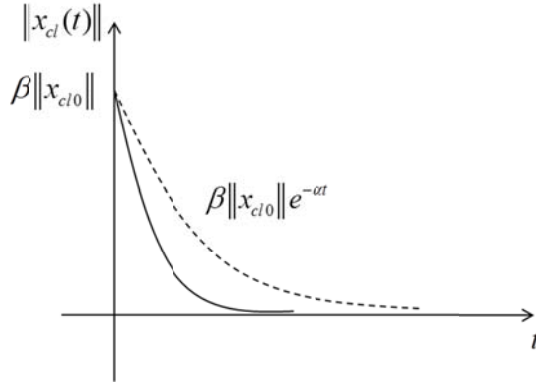


Figure 4.4: Performance with decay rate

In this thesis, we will establish exponential stability of the above time-varying system by seeking a quadratic Lyapunov function $V(x_{cl}) = x_{cl}^T P x_{cl}$. In this case, we say that this system is quadratically stable. From Lyapunov theory [28], the system

$$\dot{x}_{cl} = A_{cl}(t)x_{cl}; A_{cl}(t) \in \{A_{cl1}, A_{cl2}, \dots, A_{clN}\}; t \geq 0; x_{cl}(0) = x_{cl0}$$

is quadratically stable if there exist symmetric, positive-definite matrices P and Q such that the time derivative of $V(x_{cl})$ along solutions to the differential equation is satisfies

$$\begin{aligned}\dot{V}(x_{cl}) &\triangleq \left. \frac{dV(x_{cl})}{dt} \right|_{\dot{x}_{cl}=A_{cl}(t)x_{cl}} \\ &= x_{cl}^T \left[A_{cl}^T(t)P + PA_{cl}(t) \right] x_{cl} \leq -x_{cl}^T Q x_{cl}; \forall t > 0, \quad \forall x_{cl} \neq 0.\end{aligned}$$

where we define $A_{cl}^T(t)P + PA_{cl}(t) \leq -Q$.

Now, to prove that quadratic stability implies exponential stability, we assume that the system is quadratically stable so that

$$\dot{V}(x_{cl}) \leq x_{cl}^T (-Q)x_{cl} \leq -\lambda_{\min}(Q) \|x_{cl}\|^2$$

and

$$\lambda_{\min}(P) \|x_{cl}\|^2 \leq V(x_{cl}) \leq \lambda_{\max}(P) \|x_{cl}\|^2$$

where λ_{\min} and λ_{\max} denote the minimum and maximum eigenvalues. Since both P and Q are positive definite,

$$\|x_{cl}\|^2 \geq \frac{V(x_{cl})}{\lambda_{\max}(P)}$$

and

$$\dot{V}(x_{cl}) \leq -\lambda_{\min}(Q) \|x_{cl}\|^2 \leq -\lambda_{\min}(Q) \frac{V(x_{cl})}{\lambda_{\max}(P)}.$$

With $\delta \triangleq \frac{\lambda_{\min}(Q)}{\lambda_{\max}(P)} > 0$, then

$$\dot{V}(x_{cl}) \leq -\delta V(x_{cl}),$$

and

$$V(x_{cl}(t)) \leq V(x_{cl0}) e^{-\delta t}.$$

For simplicity, let $\delta = 2\alpha$, so that

$$V(x_{cl}(t)) \leq V(x_{cl0}) e^{-2\alpha t}.$$

Again, since

$$\lambda_{\min}(P)\|x_{cl}\|^2 \leq V(x_{cl}),$$

we get

$$\lambda_{\min}(P)\|x_{cl}(t)\|^2 \leq V(x_{cl0})e^{-2\alpha t},$$

so

$$\lambda_{\min}(P)\|x_{cl}(t)\|^2 \leq \lambda_{\max}(P)\|x_{cl0}\|^2 e^{-2\alpha t}.$$

Then,

$$\|x_{cl}(t)\|^2 \leq \frac{\lambda_{\max}(P)}{\lambda_{\min}(P)}\|x_{cl0}\|^2 e^{-2\alpha t}$$

and

$$\|x_{cl}(t)\| \leq \sqrt{\frac{\lambda_{\max}(P)}{\lambda_{\min}(P)}}\|x_{cl0}\| e^{-\alpha t}.$$

Letting β denote $\sqrt{\frac{\lambda_{\max}(P)}{\lambda_{\min}(P)}}$ gives

$$\|x_{cl}(t)\| \leq \beta\|x_{cl0}\| e^{-\alpha t},$$

which proves exponential stability.

Summarizing, if $\dot{x}_{cl} = A_{cl}(t)x_{cl}$ is quadratically stable, then it is exponentially stable for arbitrary measurable functions $\lambda_i(t)$.

Note that exponential stability does not imply quadratic stability. For example, from [26] the system

$$\dot{x} = A(t)x; A(t) \in \{A_1, A_2\}$$

where

$$A_1 = \begin{bmatrix} -1 & -1 \\ 1 & -1 \end{bmatrix} \quad \text{and} \quad A_2 = \begin{bmatrix} -1 & -a \\ 1/a & -1 \end{bmatrix}.$$

is exponentially stable, however, there is no positive definite quadratic Lyapunov function to satisfy the quadratic stability criterion for $3 + \sqrt{8} < a < 10$.

4.5 Robust performance analysis and examples

From Section 4.4, we showed that quadratic stability implies exponential stability so that

$$\|x(t)\| \leq \beta \|x_0\| e^{-\alpha t}; \alpha, \beta > 0$$

where $\beta = \sqrt{\frac{\lambda_{\max}(P)}{\lambda_{\min}(P)}}$. This shows that the response of the closed-loop system has a time constant which is no greater than $\frac{1}{\alpha}$ days. Notice that exponential stability actually indicates how fast the system responds - time constant provides an upper bound of the speed of response, and this is a performance of such system.

In this time-varying case, where we assume each RBC is endowed with a lifespan from a distribution chosen from a predetermined collection, this performance of response is guaranteed for all admissible time-varying lifespan distributions $l(t, \tau) \in \{l_{k_1, \bar{\tau}_1}(\tau), l_{k_2, \bar{\tau}_2}(\tau), \dots, l_{k_N, \bar{\tau}_N}(\tau)\}$.

In this section, we will first link quadratic stability with robust performance, i.e., finding the largest α such that

$$\|x(t)\| \leq \beta \|x_0\| e^{-\alpha t}$$

for all admissible time-varying lifespans. Moreover, we would like to explore how this best $\frac{1}{\alpha}$ (time constant) is affected by the parameters of the time-varying family of lifespan distributions as well as the parameters of the PI controller.

4.5.1 Robust performance

In our time-varying case, the system is described by

$$\dot{x}_{cl} = A_{cl}(t)x_{cl}; A_{cl}(t) \in \{A_{cl1}, A_{cl2}, \dots, A_{clN}\}, x_{cl}(0) = x_{cl0}$$

where x_{cl} is state of the closed-loop system. Recall that this system is quadratically stable if there exists a quadratic Lyapunov function $V(x_{cl}) = x_{cl}^T P x_{cl}$, where P is a symmetric and positive-definite matrix such that

$$\dot{V}(x_{cl}(t)) = x_{cl}^T [A_{cl}^T(t)P + PA_{cl}(t)] x_{cl} \leq -x_{cl}^T Q x_{cl}; \forall x_{cl}(t) \neq 0, \forall t > 0.$$

Now consider bounding this Lyapunov equation as follows:

$$A_{cl}^T(t)P + PA_{cl}(t) \leq -2\alpha P; \quad \alpha > 0.$$

Then,

$$x_{cl}^T \left[A_{cl}^T(t)P + PA_{cl}(t) \right] x_{cl} \leq -2\alpha x_{cl}^T P x_{cl},$$

which is equivalent to

$$\dot{V}(x_{cl}) \leq -2\alpha V(x_{cl}),$$

and

$$V(x_{cl}(t)) \leq V(x_{cl0})e^{-2\alpha t}.$$

Now, following the development in Section 4.4, we immediately obtain

$$\|x_{cl}(t)\| \leq \beta \|x_{cl0}\| e^{-\alpha t}.$$

Since $A_{cl}(t) \in \{A_{cl1}, A_{cl2}, \dots, A_{clN}\}$, it is obvious that

$$A_{cl}^T(t)P + PA_{cl}(t) \leq -2\alpha P; \quad t \geq 0$$

means that

$$A_{cli}^T P + PA_{cli} \leq -2\alpha P; \quad i = 1, 2, \dots, N.$$

As a result, finding the largest α such that

$$A_{cli}^T P + PA_{cli} \leq -2\alpha P; \quad i = 1, 2, \dots, N$$

could be transferred into the problem of determining the largest α such that

$$\|x_{cl}(t)\| \leq \beta \|x_{cl0}\| e^{-\alpha t}$$

for all admissible time-varying lifespan distributions, but not vice versa.

In this thesis, we will use Mathwork's LMI toolbox to establish the quadratic stability and exponential stability of the time-varying AMCS:

$$\dot{x}_{cl} = A_{cl}(t)x_{cl}; \quad A_{cl}(t) \in \{A_{cli}, i = 1, 2, \dots, N\}.$$

To begin, we first note that quadratic stability of the above is equivalent to finding a symmetric positive definite P such that

$$A_{cli}^T P + PA_{cli} \leq -Q, \quad i = 1, 2, \dots, N.$$

Indeed,

$$A_{cl}^T(t)P + PA_{cl}(t) \leq -Q, \quad \forall t \geq 0; A_{cl}(t) \in \{A_{cl1}, A_{cl2}, \dots, A_{clN}\}$$

if and only if $A_{cli}^T P + PA_{cli} \leq -Q$ holds for $i = 1, 2, \dots, N$.

The LMI toolbox commands for establishing quadratic stability and exponential stability are as follows. First, the command

$$P = \text{lmivar}(1, [n \ 1])$$

declares matrix P to be the primary LMI variable; i.e., a symmetric matrix of dimension n . Second, the desired positive definiteness of P is imposed with

$$\text{lmitem}([-1 \ 1 \ 1 \ P], 1, 1).$$

In determining the largest α such that $A_{cli}^T P + PA_{cli} \leq -2\alpha P$ by finding the minimum $-\alpha$ and corresponding P , LMI toolbox constructs the N Lyapunov function $A_{cli}^T P + PA_{cli} \leq -\alpha P$ via:

$$\text{lmitem}([n \ 1 \ 1 \ P], 1, \text{Acln}, 's')$$

and

$$\text{lmitem}([-n \ 1 \ 1 \ P], 1, 1).$$

Then, the LMI toolbox command “gevp” is called to solve $A_{cli}^T P + PA_{cli} \leq -\alpha P$; i.e.,

$$[\alpha, \text{popt}] = \text{gevp}(\text{lmis}, 2)$$

where “alpha” is the computed minimum $-\alpha$ and “popt” returns the Lyapunov matrix P . The P matrix in a normal form³ is given by command

$$P = \text{dec2mat}(\text{lmis}, \text{popt}, P)$$

if the returned $-\alpha < 0$. Also, matrix Q could be computed via α and P . Finally, the least estimate of the AMCS’s time-constant is given by $\frac{1}{\alpha}$ days.

4.5.2 Illustrative example

We now give an example of establishing the exponential stability of the AMCS

³ “popt” returns a P matrix with decision variables in the LMI solver, the P matrix in LMIs are of matrix variables, thus “dec2mat” is used to compute corresponding matrix values, given decision values of P .

$$\dot{x}_{cl} = A_{cl}(t)x_{cl}; \quad x_{cl}(0) = x_{cl_0}; \quad A_{cl}(t) \in \{A_{cl1}, A_{cl2}\}$$

where

$$l_{k_i, \bar{\tau}_i}(\tau) = \frac{k_i^{k_i}}{\bar{\tau}_i^{k_i}} \frac{1}{\Gamma(k_i)} \tau^{k_i-1} e^{-\frac{k_i \tau}{\bar{\tau}_i}}; \quad i = 1, 2;$$

$$\bar{\tau}_1 = 80; \quad \bar{\tau}_2 = 60; \quad k_1 = 2; \quad k_2 = 3;$$

and

$$K_p = 0.005; \quad K_l = 0.0001.$$

We now invoke Mathwork's LMI toolbox command 'gevp' to find the largest α such that

$$P > 0$$

$$A_{cli}^T P + P A_{cli} < -2\alpha P, \quad i = 1, 2.$$

The matrices A_{cl1} and A_{cl2} are:

$$A_{cl1} = \begin{bmatrix} -0.0138 & 0.0112 & 0 & 0 & 0 & -1.0820 & 0 \\ -0.0112 & -0.0362 & 0 & 0 & 0 & -0.4133 & 0 \\ 0 & 0 & -0.0188 & -0.0190 & 0.0056 & 0 & 0 \\ 0 & 0 & 0.0190 & -0.0434 & 0.0300 & 0 & 0 \\ 0 & 0 & 0.0056 & -0.0300 & -0.0879 & 0 & 0 \\ 0.0015 & -0.0006 & 0.0016 & 0.0007 & -0.0002 & -0.2857 & 0.2857 \\ 0.0001 & -0.0000 & 0.0001 & 0.0001 & -0.0000 & 0 & 0 \end{bmatrix};$$

$$A_{cl2} = \begin{bmatrix} -0.0138 & 0.0112 & 0 & 0 & 0 & 0 & 0 \\ -0.0112 & -0.0362 & 0 & 0 & 0 & 0 & 0 \\ 0 & 0 & -0.0188 & -0.0190 & 0.0056 & -1.1100 & 0 \\ 0 & 0 & 0.0190 & -0.0434 & 0.0300 & 0.5100 & 0 \\ 0 & 0 & 0.0056 & -0.0300 & -0.0879 & 0.1670 & 0 \\ 0.0015 & -0.0006 & 0.0016 & 0.0007 & -0.0002 & -0.2857 & 0.2857 \\ 0.0001 & -0.0000 & 0.0001 & 0.0002 & -0.0000 & 0 & 0 \end{bmatrix}.$$

Using Matlab's 'gevp' command as previously discussed, it is determined that this system possesses the quadratic Lyapunov function $x_{cl}^T P x_{cl}$ where

$$P = 1.0e - 004 *$$

$$\begin{bmatrix} 0.0013 & 0.0012 & 0.0015 & -0.0003 & -0.0008 & -0.0374 & 0.0940 \\ 0.0012 & 0.0017 & 0.0015 & -0.0006 & -0.0008 & 0.0270 & 0.0406 \\ 0.0015 & 0.0015 & 0.0017 & -0.0004 & -0.0009 & -0.0376 & 0.1040 \\ -0.0003 & -0.0006 & -0.0004 & 0.0003 & 0.0002 & -0.0275 & 0.0063 \\ -0.0008 & 0.0008 & -0.0009 & 0.0002 & 0.0009 & 0.0039 & -0.0443 \\ -0.0374 & 0.0270 & -0.0376 & -0.0275 & 0.0039 & 8.3101 & -8.1048 \\ 0.0940 & 0.0406 & 0.1040 & 0.0063 & -0.0443 & -8.1048 & 10.8220 \end{bmatrix}$$

$$Q = 1.0e - 0007 *$$

$$\begin{bmatrix} 0.0072 & 0.0067 & 0.0082 & -0.0016 & -0.0044 & -0.2039 & 0.5131 \\ 0.0067 & 0.0094 & 0.0079 & -0.0034 & -0.0046 & 0.1475 & 0.2216 \\ 0.0082 & 0.0079 & 0.0095 & -0.0020 & -0.0051 & -0.2050 & 0.5676 \\ -0.0016 & -0.0034 & -0.0020 & 0.0017 & 0.0013 & -0.1500 & 0.0341 \\ -0.0044 & -0.0046 & -0.0051 & 0.0013 & 0.0051 & 0.0215 & -0.2418 \\ -0.2039 & 0.1475 & -0.2050 & -0.1500 & 0.0215 & 45.3542 & -44.2339 \\ 0.5131 & 0.2216 & 0.5676 & 0.0341 & -0.2418 & -44.2339 & 59.0634 \end{bmatrix}$$

We verify that

$$\lambda_{\min}(P) = 1.0130e-010$$

$$\lambda_{\min}(Q) = 5.5287e-013$$

so that P and Q are indeed positive-definite, implying that the AMCS is quadratically stable and exponentially stable. The returned $\alpha = 0.0055$, thus for the uncertain family of time-varying lifespan distributions

$$l(t, \tau) \in \{l_{k_1, \bar{\tau}_1}(\tau), l_{k_2, \bar{\tau}_2}(\tau)\};$$

$$\bar{\tau}_1 = 80; \quad \bar{\tau}_2 = 60; \quad k_1 = 2; \quad k_2 = 3;$$

and

$$C_a(s) = \frac{0.005(s + 0.02)}{s},$$

the closed-loop response of the AMCS satisfy

$$\frac{1}{\alpha} = \frac{1}{0.0055} \approx 183 \text{ days,}$$

this indicates that the response of the system after dosing is faster than at least 183 days.

4.5.3 Impact of parameters of lifespans and controller

In this section we do a modest parametric study to observe the impact that parameters describing the time-varying family of lifespan distributions and parameters of the PI-AMP $C_a(s)$ have on the closed-loop time constant as computed in the previous section. For simplicity, we continue to study the case of $N = 2$ such that

$$l(t, \tau) \in \{l_{k_1, \bar{\tau}_1}(\tau), l_{k_2, \bar{\tau}_2}(\tau)\}$$

is parameterized by the numbers $k_1, k_2, \bar{\tau}_1, \bar{\tau}_2$. The PI-AMP

$$C_a(s) = K_p + \frac{K_I}{s}$$

can be re-parameterized as

$$C_a(s) = \frac{K(s+z)}{s}$$

where $K = K_p$ is the gain and $z = \frac{K_I}{K_p}$ is the zero of the PI-AMP. Here we fix

$z = 0.02$ so that the gain K is the only parameter we study for the PI controller. We will explore the effects that the set of parameters $\{k_1, k_2, \bar{\tau}_1, \bar{\tau}_2, K\}$ have on the AMCS' time constant.

Example 1:

In our first example, we fix

$$\bar{\tau}_2 = 80; \quad k_1 = k_2 = 2; \quad z = 0.02;$$

and compute AMCS time constant over parameters

$$\bar{\tau}_1 \in [50, 120]; \quad K = \{0.005, 0.01, 0.02, 0.04, 0.08\}.$$

The results are shown in Figure 4.5.

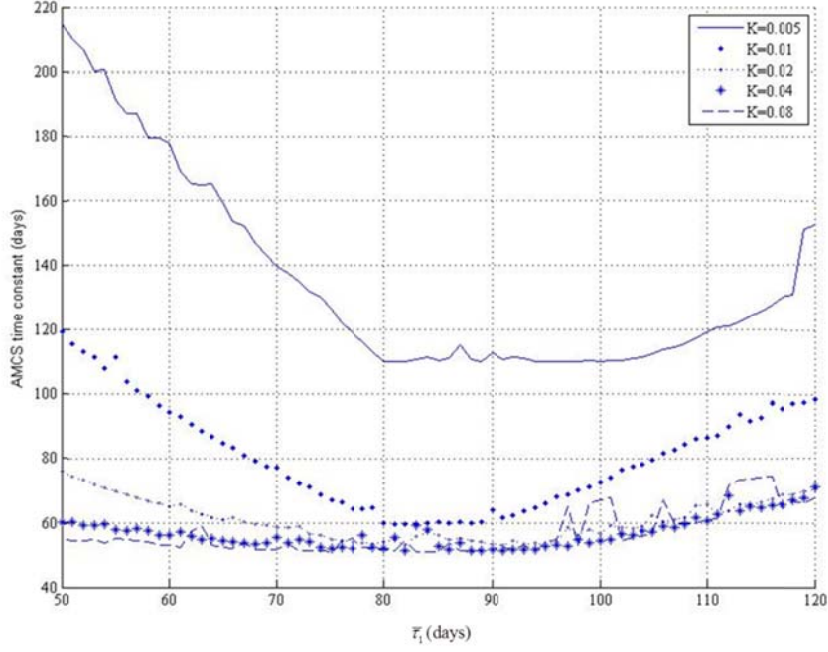


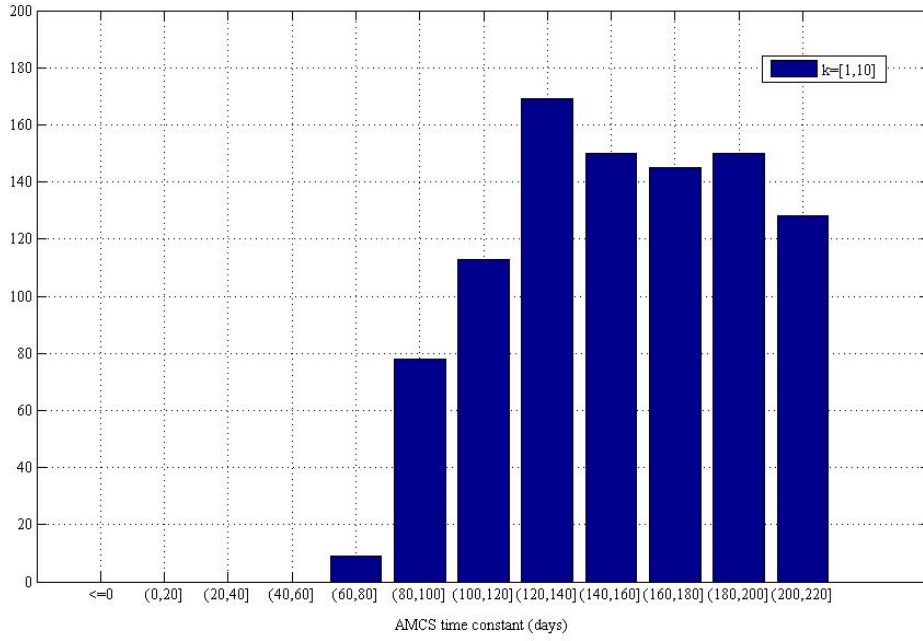
Figure 4.5: AMCS time constant $\left(\frac{1}{\alpha}\right)$ vs. pool mean lifespan $(\bar{\tau}_1)$ parameterized by gain of the PI-AMP (K)

Several conclusions in Figure 4.5 are made. First, this time-varying AMCS is exponentially stable for all parameters considered, for there is no negative value of time constant. Second, the AMCS time constant decreases with increasing K ; i.e., as the PI-AMP becomes more aggressive.

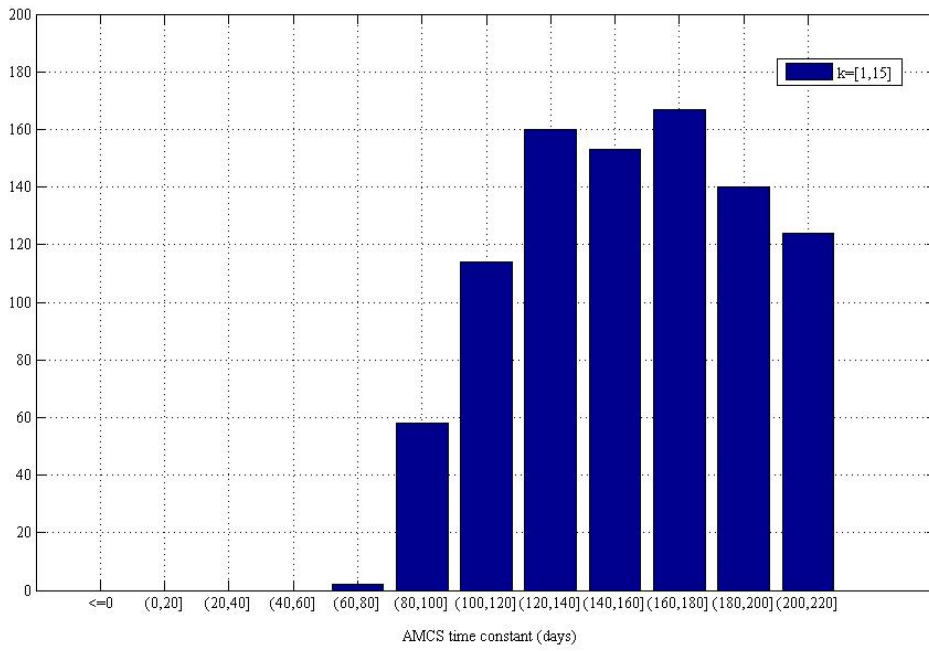
Example 2:

The next example is aimed at studying the impact on AMCS stability by the order of gamma distribution k .

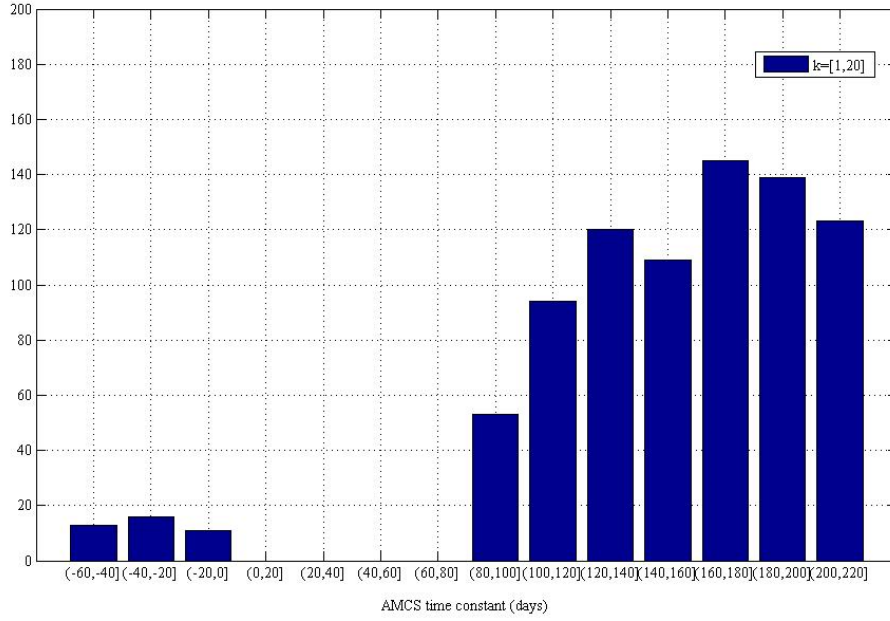
In the case of $N=2$, we keep $(\bar{\tau}_1, \bar{\tau}_2)$ in the range of $[50, 120]$. Then we randomly choose (k_1, k_2) from uniform distributions over $[1, 10]$, $[1, 15]$ and $[1, 20]$ respectively, with the parameters of the PI-AMP fixed at $K = 0.005$ and $z = 0.02$. Figure 4.6 is a histogram of the AMCS time-constant, where the x-axis is the AMCS time constants.



(a)



(b)



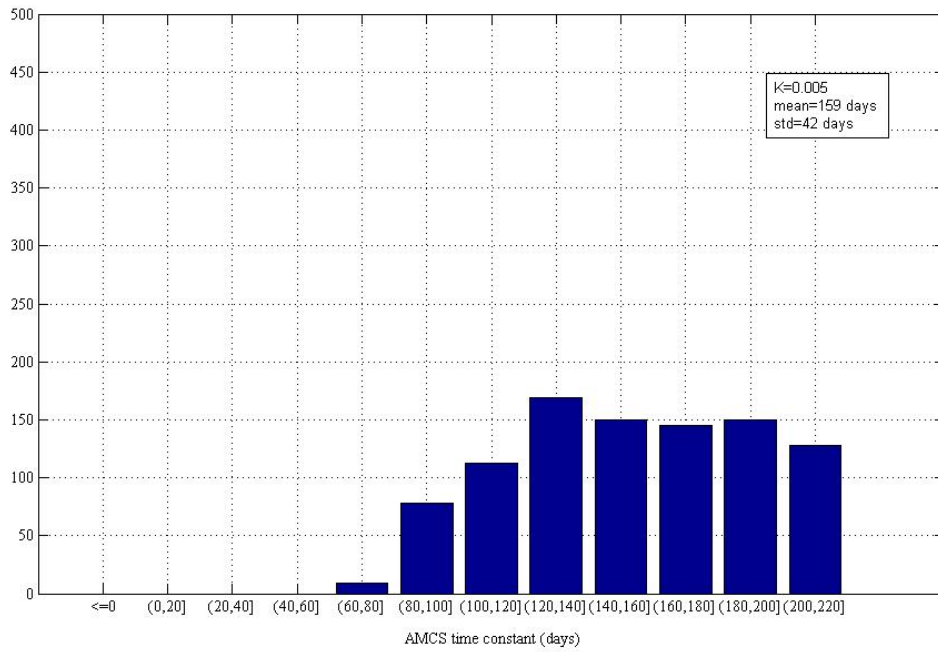
(c)

Figure 4.6: distribution of AMCS time constant $\left(\frac{1}{\alpha}\right)$ parameterized over pool mean lifespan $(\bar{\tau})$ and order of lifespan distribution (k)

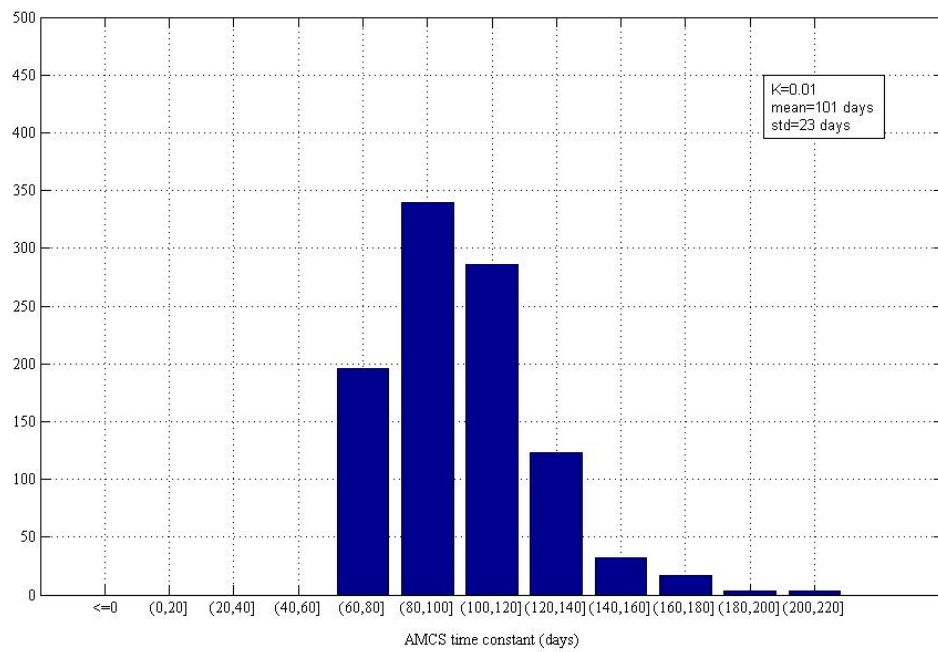
The plot in Figure 4.6 shows that the AMCS loses quadratic stability for large values of k_1 and k_2 .

Example 3:

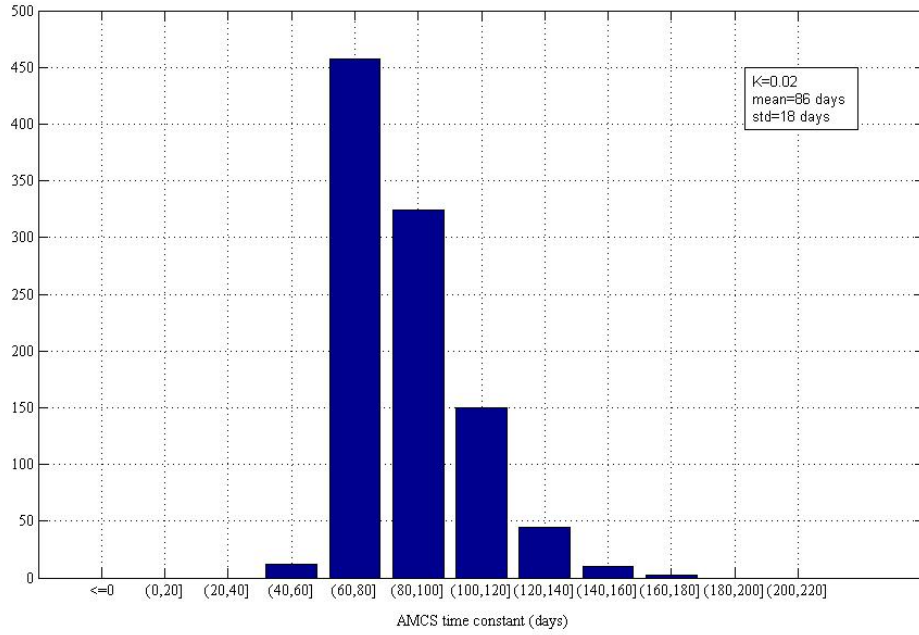
In this example we consider parametric variations over several values of PI-AMP gain K . The objective is to observe the impact of the PI-AMP's aggressiveness on the distribution of AMCS time constant resulting from variations in the time-varying RBC lifespan parameters $\bar{\tau}$ randomly choose from $[50,120]$ and k from $[1,10]$.



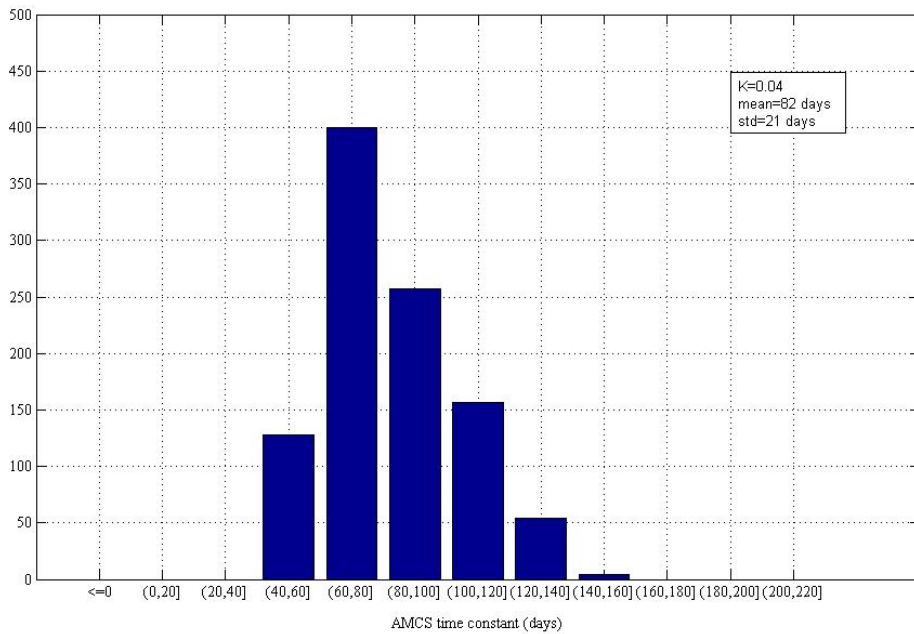
(a)



(b)



(c)



(d)

Figure 4.7: distribution of AMCS time constant $\left(\frac{1}{\alpha}\right)$ parameterized over pool mean lifespan $(\bar{\tau})$, order of lifespan distribution (k) and PI-AMP gain (K)

It can be seen that both the mean and standard derivation of the time constant decreases when PI controller parameter K increases, meaning that as K increases, the system tends to respond faster. This is also similar with the results in Figure 4.5.

CHAPTER 5

CONCLUSIONS

In this thesis, we focused on building models of the RBC lifespan distribution uncertainty and analyzing their impact on the AMCS. We first considered the general case of RBC pool dynamics, regarding it as a compartmental model with $\bar{k}_{in}(t)$ denoting the rate of newly-born RBCs entering the pool, with $l(t, \tau)$ as the time-varying lifespan (τ) distribution of the cells and with $Hgb(t)$ the pool's output describing hemoglobin level. The general dynamic of the RBC pool was given by the differential equation

$$\dot{Hgb}(t) = \bar{k}_{in}(t) - \int_0^t \bar{k}_{in}(t-\tau)l(\tau, t-\tau)d\tau .$$

For the time-invariant case where $l(t, \tau) \equiv l(\tau)$, the RBC pool could be represented by its transfer function

$$H(s) \triangleq \frac{Hgb(s)}{K_{in}(s)} = \frac{1-L(s)}{s}$$

where L is the Laplace transform of $l(\tau)$.

In chapter 1 we proved some basic properties of $H(s)$, namely:

- i) $H(s)$ is BIBO stable.
- ii) $H(0) = \bar{\tau}$: this property shows the RBC pool dynamics contribution to the open-loop gain of the AMCS.
- iii) $|H(j\omega)| \leq \frac{2}{\omega}$ and $|H(j\omega)| \leq \bar{\tau}$: this property demonstrates that the bandwidth of the RBC pool is bounded by $\frac{2}{\bar{\tau}}$ rad/day, also, the time constant of response will always be greater than $\frac{\bar{\tau}}{2}$ days.

Finally, future research may consider formally establishing the passivity of the RBC pool dynamic, and exploring this property in terms of uncertainty and AMCS performance.

In chapter 3, we first considered a time-invariant model for the RBC lifespan distribution uncertainty which allowed lifespan variations amongst the population, and focused on the family of gamma distributions described by

$$l_{k,\bar{\tau}}(\tau) = \frac{k^k}{\bar{\tau}^k} \frac{1}{\Gamma(k)} \tau^{k-1} e^{-\frac{k\tau}{\bar{\tau}}},$$

its Laplace transform is $L(s) = \frac{1}{\left(\frac{s\bar{\tau}}{k} + 1\right)^k}$ and associated RBC pool dynamic

$H_k(s) = \frac{1 - L_k(s)}{s}$. We chose a multiplicative model of uncertainty with nominal model

$$H_1(s) = \frac{\bar{\tau}}{s\bar{\tau} + 1},$$

and the multiplicative error is $\Delta(s) \triangleq \frac{H_k(j\omega)}{H_1(j\omega)} - 1$. We then conjectured a tight bound

(independent of order k) on this error

$$|\Delta(j\omega)| \leq \left| \frac{1 - (1 + j\omega\bar{\tau})e^{-j\omega\bar{\tau}}}{j\omega\bar{\tau}} \right|.$$

This conjecture is still open and we showed the looser bound (see Appendix, Figure A.1):

$$|\Delta(j\omega)| \leq \begin{cases} \frac{\sqrt{30}}{9} \cdot \omega\bar{\tau}; & 0 \leq \omega\bar{\tau} < 1 \\ 1 + \frac{2}{\omega\bar{\tau}}; & \omega\bar{\tau} \geq 1 \end{cases}.$$

The primary implication of these bounds is that they provide useful constraints on the AMCS' complementary sensitivity to achieve robust performance; see Figure 3.6 - 3.8. One future direction in this inquiry is to consider multiplicative error models arising from different choices of nominal RBC dynamics. In this thesis we solely considered $H_1(s)$ as nominal. However, it may make sense to choose $H_k(s)$ for some given k , as nominal, and then the question on a suitable bound on the multiplicative error can be asked.

In chapter 4, we studied a time-varying model of RBC lifespan distributions

wherein the lifespan for each new cell is chosen according to a choice of distribution from a finite collection of time-invariant distributions:

$$l(t, \tau) \in \{l_1(\tau), l_2(\tau), \dots, l_N(\tau)\}.$$

A key definition of this model is the separation

$$l(t, \tau) = \begin{bmatrix} \lambda_1(t) & \lambda_2(t) & \cdots & \lambda_N(t) \end{bmatrix} \begin{bmatrix} l_{k_1, \bar{\tau}_1}(\tau) \\ l_{k_2, \bar{\tau}_2}(\tau) \\ \vdots \\ l_{k_N, \bar{\tau}_N}(\tau) \end{bmatrix}$$

where $\lambda_i(t)$ is time varying and $\sum_{i=1}^N \lambda_i(t) = 1$. This allows us to express the AMCS in

a standard form:

$$\dot{x}_{cl} = A_{cl}(t)x_{cl}; A_{cl}(t) \in \{A_{cl1}, A_{cl2}, \dots, A_{clN}\}.$$

Within this framework, we conducted Matlab experiments to analyze the impact on AMCS performance due to a PI-AMP's gain and to different collections of distributions. We saw that time variant in mean lifespan did not adversely affect stability; the gamma distribution order could cause instability for large ranges. The main analytical tool used for these time-varying dynamical systems was quadratic Lyapunov functions. Future research could consider other Lyapunov candidates such as polytopic Lyapunov functions which may be better suited to this class of uncertainties which do fall into the large category of polytopic uncertainty [27].

APPENDIX

PROOF FOR THEOREM 3.1

A Proof for Theorem 3.1

Define
$$Z_k = \frac{j\omega\bar{\tau} + 1}{\left(\frac{j\omega\bar{\tau}}{k} + 1\right)^k}$$

Lemma 1: For $0 \leq \omega\bar{\tau} < 1$ and positive integer k :

$$|Z_k|^2 \leq 1 + \left(1 - \frac{1}{k}\right) \cdot (\omega\bar{\tau})^2$$

$$\text{Re}(Z_k) \geq 1 + \left(1 - \frac{1}{k}\right) \cdot \frac{(\omega\bar{\tau})^2}{2} - \frac{(k-1)(k+1)(k+2)}{8k^3} \cdot (\omega\bar{\tau})^4$$

hence

$$|1 - Z_k|^2 \leq \frac{10}{27} \cdot (\omega\bar{\tau})^4.$$

Proof for Lemma 1:

Since $Z_k = \frac{j\omega\bar{\tau} + 1}{\left(\frac{j\omega\bar{\tau}}{k} + 1\right)^k}$, in particular $Z_1 = 1$, then $\left|\frac{H_k}{H_1} - 1\right|^2 = \left|\frac{1 - Z_k}{j\omega\bar{\tau}}\right|^2 = \frac{|1 - Z_k|^2}{(\omega\bar{\tau})^2}$.

Also, Z_k is a complex number,

$$|1 - Z_k|^2 = 1 + |Z_k|^2 - 2\text{Re}(Z_k).$$

Now using the Taylor expansion, it is easy to get that around $\omega\bar{\tau} = 0$ when $0 \leq \omega\bar{\tau} < 1$,

$$|Z_k|^2 = 1 + \sum_{n=1}^{\infty} \frac{(-1)^{n-1} (k+n-2)! (n \cdot k + n - 1)}{n \cdot k^{2n} \cdot (k-2)! (n-1)!} \cdot \frac{(\omega\bar{\tau})^{2n}}{n!},$$

$$-2\text{Re}(Z_k) = -2 - 2 \sum_{n=1}^{\infty} (-1)^{n-1} (2n-1) \cdot \frac{(k+2n-2)!}{k^{2n} \cdot (k-2)!} \cdot \frac{(\omega\bar{\tau})^{2n}}{(2n)!}.$$

The Taylor Inequality gives

$$|Z_k|^2 \leq 1 + \left(1 - \frac{1}{k}\right) \cdot (\omega\bar{\tau})^2,$$

$$-2\operatorname{Re}(Z_k) \leq -2 - \left(1 - \frac{1}{k}\right) \cdot (\omega\bar{\tau})^2 + \frac{(k-1)(k+1)(k+2)}{4k^3} \cdot (\omega\bar{\tau})^4,$$

this gives

$$\begin{aligned} |1 - Z_k|^2 &\leq 1 + 1 + \left(1 - \frac{1}{k}\right) \cdot (\omega\bar{\tau})^2 - 2 - \left(1 - \frac{1}{k}\right) \cdot (\omega\bar{\tau})^2 + \frac{(k-1)(k+1)(k+2)}{4k^3} \cdot (\omega\bar{\tau})^4 \\ &= \frac{(k-1)(k+1)(k+2)}{4k^3} \cdot (\omega\bar{\tau})^4. \end{aligned}$$

For $k \geq 3$, the function $f(k) = \frac{(k-1)(k+1)(k+2)}{4k^3}$ has

$$\begin{aligned} f'(k) &= \left[\frac{(k-1)(k+1)(k+2)}{4k^3} \right]' \\ &= -\frac{1}{2k^2} \cdot \frac{k^2 - k - 3}{k^2} \end{aligned}$$

so when $k \geq 3$, we get

$$f'(k) > 0, \quad f(k) \geq f(3) = \frac{10}{27},$$

the result is that when $k \geq 3$,

$$|1 - Z_k|^2 \leq \frac{10}{27} \cdot (\omega\bar{\tau})^4,$$

then

$$\left| \frac{H_k}{H_1} - 1 \right|^2 = \frac{|1 - Z_k|^2}{(\omega\bar{\tau})^2} \leq \frac{\frac{10}{27} \cdot (\omega\bar{\tau})^4}{(\omega\bar{\tau})^2} = \frac{10}{27} \cdot (\omega\bar{\tau})^2,$$

so the upper bound is given by

$$\left| \frac{H_k}{H_1} - 1 \right| \leq \sqrt{\frac{10}{27} \cdot (\omega\bar{\tau})^2} = \frac{\sqrt{30}}{9} \cdot \omega\bar{\tau}.$$

This upper bound also holds when $k = 1$ and 2 :

$$\text{For } k = 1, \quad \left| \frac{H_k}{H_1} - 1 \right| = 0 \leq \frac{\sqrt{30}}{9} \cdot \omega\bar{\tau}; \quad 0 \leq \omega\bar{\tau} < 1.$$

For $k = 2$,

$$\left| \frac{H_k}{H_1} - 1 \right| = \frac{\frac{\omega\bar{\tau}}{4}}{\sqrt{(\omega\bar{\tau})^2 + \left[1 - \frac{(\omega\bar{\tau})^2}{4}\right]^2}} = \frac{\omega\bar{\tau}}{(\omega\bar{\tau})^2 + 4},$$

it is easy to compare $\frac{\omega\bar{\tau}}{(\omega\bar{\tau})^2 + 4}$ and $\frac{\sqrt{30}}{9} \cdot \omega\bar{\tau}$, that

$$\frac{\omega\bar{\tau}}{(\omega\bar{\tau})^2 + 4} \leq \frac{\sqrt{30}}{9} \cdot \omega\bar{\tau}; \quad 0 \leq \omega\bar{\tau} < 1.$$

As a result, it is true for all $0 \leq \omega\bar{\tau} < 1$ and all integer $k > 0$ that

$$\left| \frac{H_k}{H_1} - 1 \right| \leq \frac{\sqrt{30}}{9} \cdot \omega\bar{\tau}.$$

Lemma 2: For $\omega\bar{\tau} \geq 1$ and all positive integer k ,

$$|1 - Z_k| \leq \omega\bar{\tau} + 2.$$

Proof for Lemma 2:

First,

$$\begin{aligned} \left| \frac{H_k}{H_1} - 1 \right| &= \left| \frac{\frac{1 - L_k(j\omega)}{j\omega}}{\frac{1 - L_1(j\omega)}{j\omega}} \right| = \left| \frac{1 - L_k(j\omega)}{1 - L_1(j\omega)} \right| \\ &= \left| \frac{1 - \frac{1}{\left(\frac{j\omega\bar{\tau} + 1}{k}\right)^k}}{1 - \frac{1}{j\omega\bar{\tau} + 1}} \right| = \left| \frac{j\omega\bar{\tau} + 1}{\left(\frac{j\omega\bar{\tau} + 1}{k}\right)^k} \right| \\ &= \frac{|1 - Z_k|}{\omega\bar{\tau}}. \end{aligned}$$

Now look at the numerator of the above result, which is

$$1 - Z_k = \int_0^\infty l_k(\tau) d\tau - \bar{\tau} \int_0^\infty \frac{dl_k(\tau)}{d\tau} e^{-j\omega\tau} d\tau - \int_0^\infty l_k(\tau) e^{-j\omega\tau} d\tau,$$

since $(l_k(\tau) e^{-j\omega\tau})' = \frac{dl_k(\tau)}{d\tau} e^{-j\omega\tau} - j\omega \cdot l_k(\tau) e^{-j\omega\tau}$

also $(l_k(\tau) e^{-j\omega\tau}) \Big|_0^\infty = \int_0^\infty \frac{dl_k(\tau)}{d\tau} e^{-j\omega\tau} d\tau - \int_0^\infty j\omega \cdot l_k(\tau) e^{-j\omega\tau} d\tau$

and

$$\begin{aligned}\int_0^{\infty} \frac{dl_k(\tau)}{d\tau} e^{-j\omega\tau} d\tau &= \left(l_k(\tau) e^{-j\omega\tau} \right) \Big|_0^{\infty} + \int_0^{\infty} j\omega \cdot l_k(\tau) e^{-j\omega\tau} d\tau \\ &= \int_0^{\infty} j\omega \cdot l_k(\tau) e^{-j\omega\tau} d\tau,\end{aligned}$$

then

$$\begin{aligned}|1 - Z_k| &= \left| \int_0^{\infty} l_k(\tau) (1 - \bar{\tau} j\omega \cdot e^{-j\omega\tau} - e^{-j\omega\tau}) d\tau \right| \\ &= \int_0^{\infty} l_k(\tau) \left| (1 - \bar{\tau} j\omega \cdot e^{-j\omega\tau} - e^{-j\omega\tau}) \right| d\tau.\end{aligned}$$

Now we know that

$$\begin{aligned}1 - \bar{\tau} j\omega \cdot e^{-j\omega\tau} - e^{-j\omega\tau} &= 1 - \bar{\tau} j\omega [\cos(\omega\tau) - j\sin(\omega\tau)] - [\cos(\omega\tau) - j\sin(\omega\tau)] \\ &= [1 - \omega\bar{\tau} \sin(\omega\tau) - \cos(\omega\tau)] + j[\sin(\omega\tau) - \omega\bar{\tau} \cos(\omega\tau)],\end{aligned}$$

because

$$\begin{aligned}& \left| 1 - \bar{\tau} j\omega \cdot e^{-j\omega\tau} - e^{-j\omega\tau} \right|^2 \\ &= [1 - \omega\bar{\tau} \sin(\omega\tau) - \cos(\omega\tau)]^2 + [\sin(\omega\tau) - \omega\bar{\tau} \cos(\omega\tau)]^2 \\ &= 2 + \omega^2 \bar{\tau}^2 - 2\omega\bar{\tau} \sin(\omega\tau) - 2\cos(\omega\tau),\end{aligned}$$

the magnitude is thus given by

$$\begin{aligned}\left| 1 - \bar{\tau} j\omega \cdot e^{-j\omega\tau} - e^{-j\omega\tau} \right| &= \sqrt{2 + \omega^2 \bar{\tau}^2 - 2\omega\bar{\tau} \sin(\omega\tau) - 2\cos(\omega\tau)} \\ &\leq \sqrt{2 + \omega^2 \bar{\tau}^2 + 2\omega\bar{\tau} + 2} \\ &\leq \sqrt{(2 + \omega\bar{\tau})^2} = 2 + \omega\bar{\tau}; \quad \omega\bar{\tau} \geq 1.\end{aligned}$$

So now go back to the equation that

$$|1 - Z_k| = \int_0^{\infty} l_k(\tau) \left| (1 - \bar{\tau} j\omega \cdot e^{-j\omega\tau} - e^{-j\omega\tau}) \right| d\tau,$$

we get

$$|1 - Z_k| \leq \int_0^{\infty} l_k(\tau) (\omega\bar{\tau} + 2) d\tau = \omega\bar{\tau} + 2,$$

so

$$\left| \frac{H_k}{H_1} - 1 \right| = \frac{|1 - Z_k|}{\omega\bar{\tau}} \leq \frac{\omega\bar{\tau} + 2}{\omega\bar{\tau}} = 1 + \frac{2}{\omega\bar{\tau}}.$$

Proof for Theorem 3.1:

The upper bound we provide for the multiplicative error is a piecewise continuous function. Using the results of Lemma 1 and Lemma 2, it is concluded that

$$\left| \frac{H_k}{H_1} - 1 \right| \leq \begin{cases} \frac{\sqrt{30}}{9} \cdot \omega \bar{\tau}; & 0 \leq \omega \bar{\tau} < 1 \\ 1 + \frac{2}{\omega \bar{\tau}}; & \omega \bar{\tau} \geq 1 \end{cases}$$

Figure A.1 is the matlab exercise for the above error upper bound.

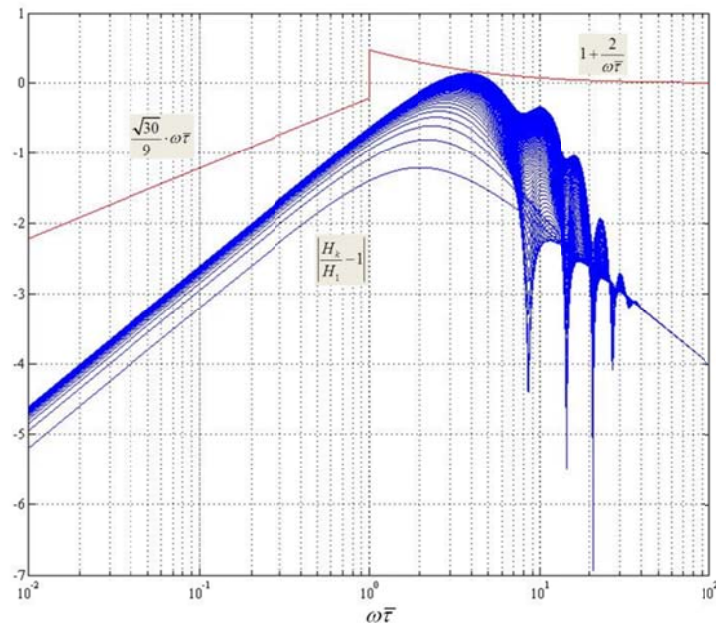


Figure A.1: Matlab example of the loser conjecture ($k = 2, 3, \dots, 100$)

BIBLIOGRAPHY

- [1] <http://faculty.stcc.edu/AandP/AP/AP2pages/Units18to20/blood/redblood.htm>
- [2] <http://www.hdcn.com/symp/06anna/01/eas/eas1.htm>
- [3] S Nurko, "Anemia in chronic kidney disease: causes, diagnosis, treatment," *Cleveland Clinic journal of medicine*, Vol. 73, No. 3, 2006:289-97
- [4] Pisoni RL, Bragg-Gresham JL, et al. "Facility-Level Interpatient Hemoglobin Variability in Hemodialysis Centers Participating in the Dialysis Outcomes and Practice Patterns Study (DOPPS): Associations With Mortality, Patient Characteristics, and Facility Practices," *American Journal of Kidney Diseases*, Vol. 57, Issue 2, 2011: 266-75
- [5] Egrie JC, Strickland TW, Lane J, et al. "Characterization and biological effects of recombinant human erythropoietin," *Immunobiology*, Vol. 72, 1986: 213-24
- [6] Wojciech Krzyzanski, Sukyung Woo, William J Jusko, "Pharmacodynamic Models for Agents that Alter Production of Natural Cells with Various Distributions of Lifespans," *Journal of Pharmacokinetics and Pharmacodynamics*, Vol. 33, No. 2, 2006:125-66
- [7] B Nichols; R. P. Shrestha, et al. "Simplification of an erythropoiesis model for design of anemia management protocols in end stage renal disease," *IEEE Engineering in Medicine and Biology Society. Conference*, 2011: 83-86
- [8] Ramakrishnan R, Cheung WK, Wacholtz MC, Minton N, Jusko WJ, "Pharmacokinetic and pharmacodynamic modeling of recombinant human erythropoietin after single and multiple doses in healthy volunteers," *J Clinical Pharmacology*, Vol. 44, No.9, 2004: 991-1002
- [9] Joanna Q. Hudson, Thomas J. Comstock, "Considerations for Optimal Iron Use for Anemia Due to Chronic Kidney Disease," *Clinical Therapeutics*, Vol. 23(10), 2001: 1637-71.
- [10] Tilman B. Drüeke et al, "Normalization of Hemoglobin Level in Patients with Chronic Kidney Disease and Anemia," *The New England Journal of Medicine*, Vol. 335, No. 20, 2006: 2071-84.
- [11] Elliott S, Pham E, Macdougall IC, "Erythropoietins: A common mechanism of action," *Experimental Hematology*, Vol. 36, 2008:1573–84.
- [12] Jerri, A.J., "Correction to The Shannon sampling theorem - Its various extensions and applications: A tutorial review", *Proceedings of the IEEE*, Vol. 67, Issue 4, 1979:695 – 695

- [13] Houpis C.H. “Refined design method for sampled-data control systems: the pseudo-continuous-time (PCT) control system design”, *Control Theory and Applications*, IEEE Proceedings D, Vol. 132, Issue 2, 1985:69-74.
- [14] Constantine H. Houpis, John J.D'Azzo, Stuart N. Sheldon, “Linear Control System Analysis and Design with Matlab”, Marcel Dekker publish, fifth edition, 2009.
- [15] R. P. Shrestha, “Modeling the lifespan of red blood cells,” [D] University of Massachusetts - Amherst, 2012
- [16] Martin H. Steinberg, Edward J. Benz Jr., Adeboye H. Adewoye, and Benjamin L. Ebert, “Hematology Basic Principles and Practice, chapter Pathobiology of the human erythrocyte and its hemoglobins”, Elsevier, Philadelphia, PA, expert premium online 5th edition, 2008.
- [17] Mark. R. Dowling, Dejan Milutinovic, Philip. D. Hodgkin, “Modelling cell lifespan and proliferation: is likelihood to die or to divide independent of age?” *Journal of the Royal Society Interface*, Vol. 2, 2005: 517-26
- [18] Kevin J. Freise, Robert L. Schmidt, John A. Widness, Peter Veng-Pedersen, “Pharmacodynamic modeling of the effect of changes in the environment on cellular lifespan and cellular response”, *Journal of Pharmacokinetics and Pharmacodynamics*, Vol. 35, 2008: 527-52
- [19] Julia Korell, Carolyn V.Coulter, Stephen B. Duffull, “A statistical model for red blood cell survival”, *Journal of Theoretical Biology*, Vol. 268, Issue 1, 2011: 39-49
- [20] Wojciech Krzyzanski. “Interpretation of transit compartments pharmacodynamics models as lifespan based indirect response models”, *Journal of Pharmacokinetics and Pharmacodynamics*, Vol. 38, Issue 2, 2011: 179-204
- [21] Mark Bebbington, Chin-Diew Lai, Ricardas Zitkiss, “Modeling human mortality using mixtures of bathtub shaped failure distributions”, *Journal of Theoretical Biology*, Vol.245, 2007:528-38
- [22] John Doyle, Bruce Francis, Allen Tannenbaum, “Feedback control theory”, Macmillan Publishing,1990
- [23] Stephen Boyd, Laurent El Ghaoui, E. Feron, and V. Balakrishnan, “Linear Matrix Inequalities in System and Control Theory”, Society for Industrial and Applied Mathematics (SIAM), 1994
- [24] Kevin J. Freise et al. “Modeling time variant distributions of cellular lifespans: increases in circulating reticulocyte lifespans following double phlebotomies in sheep”, *Journal of Pharmacokinetics and Pharmacodynamics*, Vol. 35(3), 2008: 285–323
- [25] P. Gahinet, A. Nemirovski, A. J. Laub, M. Chilali, “LMI Control Toolbox: For use with MATLAB, User’s guide”, The MathWorks, version 1, 1995

- [26] Wijesuriya P. Dayawansa, C. F. Martin, "A Converse Lyapunov Theorem for a Class of Dynamical Systems which Undergo Switching", IEEE transactions on automatic control, Vol. 44(4), 1999: 751-60
- [27] Alireza Karimi; Hamid Khatibi; Roland Longchamp, "Robust control of polytopic systems by convex optimization", Automatica, Vol.43, Issue 8, 2007: 1395-1402
- [28] Daniel Liberzon , A. Stephen Morse, "Benchmark problems in stability and design of switched system", IEEE Control Systems Magazine, Vol.19, 1999:1-22
- [29] Unger EF, Thompson AM, Blank MJ, Temple R, "Erythropoiesis stimulating agents - time for a reevaluation", New England Journal of Medicine, Vol. 362(3), 2010:189-92
- [30] E.A. Coddington, N. Levinson, "Theory of ordinary Differential Equations", McGraw-Hill, 1955
- [31] M.J. Corless, M.J., G. Leitmann, "Continuous state feedback guaranteeing uniform ultimate boundedness for uncertain dynamic systems", IEEE transaction on automatic control, Vol.26, Issue 5, 1981: 1139-44
- [32] Katalin M. Hangos, József Bokor, Gábor Szederkényi, "Analysis and Control of Nonlinear Process Systems", Springer, 2004